2024-08

Assessment of Mpanda groundwater contamination and the effectiveness of the baobab seeds-derived biochar for iron removal from groundwater

Mkelemi, Magdalena

NM-AIST

ASSESSMENT OF MPANDA GROUNDWATER CONTAMINATION AND THE EFFECTIVENESS OF THE BAOBAB SEEDS-DERIVED BIOCHAR FOR IRON REMOVAL FROM GROUNDWATER

Magdalena Mkelemi

A Dissertation Submitted in Partial Fulfilment of the Requirements for the Master's Degree in Hydrology and Water Resources Engineering of the Nelson Mandela African Institution of Science and Technology, Arusha, Tanzania
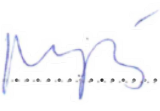
August, 2024

ABSTRACT

Groundwater in Mpanda District, Tanzania, faces excessive iron content, causing a reddish-brown colouration due to oxidized iron species. The present study evaluated Mpanda groundwater contamination and the effectiveness of baobab seeds-derived biochar for iron removal from groundwater. First, the physicochemical quality of groundwater was investigated. Nineteen boreholes were randomly selected for assessment, with samples collected in rainy and dry seasons. The study revealed significant variations in groundwater quality both between seasons and among boreholes. Temperature, total dissolved solids, electrical conductivity, lead, iron and manganese exceeding World Health Organization and Tanzania Bureau of Standards limits in some boreholes; necessitating water treatment for human use. Second, the effectiveness of baobab seeds-derived biochar for iron removal from groundwater was assessed. Baobab seeds, were sun-dried, oven dried at 105 ºC, carbonized at 700 ºC, and ground into fine powder. The influence of pH, time, temperature and dose of biochar on the iron removal from groundwater was assessed. Six 1000 mL beakers were filled with groundwater and adsorbent doses of 0.6 g/L, 1.2 g/L, 1.8 g/L, 2.4 g/L, and 3.0 g/L were added into five beakers with the sixth serving as a control. The highest removal efficiency of iron was observed within 5.0-8.0 pH range. Over time, the removal efficiency increased to 87% at 120 minutes and 3.0 g dose, with an initial iron concentration of 5.88 mg/L and residual concentration of 0.76 mg/L. Baobab seeds-derived biochar showed promising efficiency in removing iron ions and is recommended for sustainable iron removal from groundwater.

DECLARATION

I, Magdalena Mkelemi, do hereby declare to the Senate of the Nelson Mandela African Institution of Science and Technology that this dissertation is my own original work and that it has neither been submitted nor being concurrently submitted for degree award in any other institution.

Signed……………………………………………………Date…………14/08/2024……………

Magdalena Mkelemi **(Candidate name)**

Signed…………….……………………………………Date …………14/08/2024……………….

Dr. Mwemezi J. Rwiza **(Supervisor 1)**

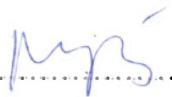Signed…………………………………………Date …………14/08/2024……………….

Dr. Grite Nelson Mwaijengo **(Supervisor 2)**

COPYRIGHT

This dissertation is copyright material protected under the Bene Convention, the Copyright Act of 1990 and other international and national enactment, in that behalf, on intellectual property. It must not be reproduced by any means, in full or in part, except for short extracts in fair dealing; for research private study, critical scholarly review or discourse with an acknowledgement, without the written permission of the office of the Deputy Vice-Chancellor for Academic, Research and Innovation on behalf of both the authors and NM-AIST.

CERTIFICATION

The undersigned certify that they have read and hereby recommend for acceptance by the Nelson Mandela African Institution of Science and Technology a Dissertation entitled: "Assessment of Mpanda Groundwater Contamination and the Effectiveness of the Baobab Seeds-Derived Biochar for Iron Removal from Groundwater" and recommend for examination in fulfillment of the requirements for Master's Degree in Hydrology and Water Resources Engineering of Nelson Mandela African Institution of Science and Technology.

Signed…………………………………………………Date …………………14/08/2024……………….

Dr. Mwemezi J. Rwiza **(Supervisor 1)**

Signed…………………………………………………Date …………………14/08/2024……………….

Dr. Grite Nelson **(Supervisor 2)**

ACKNOWLEDGEMENTS

DEDICATION

I dedicate this dissertation to the memory of my cherished parents, Mr. Juma Feruzi Mkelemi and Imakulata Noel Marufa, whose unwavering love and support continue to inspire me. Though they are no longer with us, their influence on my life and academic journey will always be cherished.

TABLE OF CONTENT

LIST OF TABLES

LIST OF FIGURES

LIST OF PLATES

LIST OF ABBREVIATIONS AND SYMBOLS

AAS   Atomic Absorption Spectrophotometer

ANOVA   Analysis of Variance

BET   Brunauer Emmett Teller

GPS   Global Positioning System

mg/kg   Milligram Per Kilogram

NM-AIST   Nelson Mandela African Institution of Science and Technology

PCA   Principal Component Analysis

RUWASA   Rural Water Supply and Sanitation Agency

SEM   Scanning Electron Microscopy

TBS   Tanzania Bureau Standards

WHO   World Health Organization

WQI   Water Quality Index

XRD   X–ray Diffraction

CHAPTER ONE

INTRODUCTION

1.1   Background to the Problem

Access to clean and safe drinking water is a fundamental human right crucial for sustaining life and promoting public health (Carrard *et al*., 2019). However, in many parts of sub-Saharan Africa, including Tanzania, this right remains unfulfilled due to significant challenges in water accessibility and quality (Abegaz & Midekssa, 2021; Es & Quaternary, 2019; Pantaleo *et al.,* 2018). The diminishing availability of surface water driven by climate change, overuse of the resource, and pollution has led to an increased dependance on groundwater sources. Groundwater has become a crucial source of water supply particularly in rural areas due to its reliability, and accessibility (Elisante & Muzuka, 2017; Pantaleo *et al.,* 2018). Groundwater is less affected by seasonal changes and provides a more consistent water supply even during droughts. Despite its advantages, groundwater is often subject to contaminations from both natural processes and anthropogenic activities (Qureshi *et al.,* 2021).

One of the most pressing issues is the contaminations by dissolved heavy metals, which can render the water unsafe for human consumption. Heavy metals in the earth's crust can dissolve in groundwater through natural geological processes or human induced processes such as leachate from waste disposal, liquid sewage, mining wastes, and industrial runoff (Edori & Kpee, 2016; Rahmanian *et al.,* 2015). Long-term consumption of water with a high concentration of heavy metals can lead to metal bioaccumulation in the body, resulting in serious health issues such as cancer, liver problems, lung diseases, and kidney disorders (Bayuo *et al.,* 2023a; Rahmanian *et al.,* 2015).

Iron (Fe) is one of the most prevalent metallic elements in groundwater, affecting its quality (bin Jusoh *et al.,* 2005; Elwakeel *et al.,* 2015). While Fe is an essential micronutrient for human health, elevated levels in drinking water can cause aesthetic problems, such as discolouration, metallic taste and stench smell, as well as infrastructure problems such as pipes and pumps clogging (Carretero & Kruse, 2015; Elwakeel *et al.,* 2015). Additionally, long-term consumption of iron-rich groundwater can cause problems like kidney failure and neurological damage (Usman *et al.,* 2021). Studies have shown that iron concentrations in groundwater exceeding 0.3 mg/L, the recommended limit by the World Health Organization (WHO) and the Tanzania Bureau of Standards (TBS), cause significant aforementioned aesthetic problems

1

(TBS, 2018; WHO, 2011). For instance, research by Hossain *et al*. (2015) reported iron concentrations ranging from 1.03 mg/L to 24.50 mg/L in Tangail Municipal, Bangladesh, while Rushdi *et al*. (2023) found average concentrations of 5.46±4.28 mg/L in Moulvibazar Sadar and 7.85±2.71 mg/L in Sreemangal.

No prior study has assessed groundwater quality in Mpanda, Tanzania. An unpublished report from the Rural Water Supply and Sanitation Agency (RUWASA) revealed high iron concentrations in groundwater samples, with colour, taste, and odour indicating iron contamination. Pure water should be colourless, odourless, clear, and palatable (Hossain *et al.,* 2015). In Mpanda, groundwater stored in tanks and buckets appeared reddish-brown (Mkelemi field survey, 2022), with similar discolouration on concrete and plumbing fixtures, a metallic taste, and a bad odour, all pointing to iron presence (Carretero & Kruse, 2015; Elwakeel *et al.,* 2015). Therefore, assessing groundwater contamination in the Mpanda district became necessary.

Various treatment methods have been used to treat contaminated groundwater including ion exchange, chlorination, filtration, coagulation and flocculation, reverse osmosis, greensand, and polyphosphates (Civardi & Tompeck, 2015; Sharma *et al.,* 2005). However, most of these methods are unreliable to implement because they require chemicals and expertise, both of which are often unaffordable or inaccessible for people in rural areas to utilize for domestic water treatment. Africa is home to numerous plant species that are rich in health-promoting compounds and can be used to purify water (Gebauer *et al.,* 2016). For example, the seeds of *Morenga oleifera* and the combined extract of its leaves and seeds have been reported as powerful natural coagulants in water purification, with little to no adverse effects on human health (Alam *et al.,* 2020; Nisar *et al.,* 2020).

Numerous studies have reported the benefits of baobab tree *(Adansonia digitata L.)* for food, medicine, and beverages (Group, 2014), but their applicability for water purification remains underexplore (Agbaka, 2020). According to Assogbadjo *et al.* (2021), the baobab plant contains many bioactive substances, with each part offering various health and nutritional advantages. Akintola *et al*. (2019) reported that, the seedlings of the baobab *(A. digitata L)* can clean contaminated soil by accumulating and distributing heavy metals from sewage sludge into their tissues.

Therefore, on the experience gained with other plant species such as moringa, and the use of baobab tree in other areas of specialization, this study intended to assess the extent of Mpanda groundwater contamination and evaluate the effectiveness of baobab seeds-derived biochar in removing Fe from groundwater. The baobab tree *(Adansonia digitata L.)* is widely distributed across sub-Saharan Africa particularly to arid and semi-arid climates regions *(Edogbanya et al.,* 2016; Gebauer *et al.,* 2016). Tanzania is one of the countries where the baobab tree is grown and cultivated. This species has been selected for its social and economic significance, marketability, accessibility to rural populations, and availability in the market.

1.2   Problem Statement

Access to clean and safe drinking water is a critical public health issue, especially in regions like Mpanda, Tanzania, where groundwater is a primary source of water for many communities. Despite its importance, no prior studies have systematically assessed the quality of groundwater in Mpanda. An unpublished RUWASA report found high iron concentrations in groundwater, with colour, taste, and odour suggesting iron contamination. Preliminary observations also noted reddish-brown discolouration, a metallic taste, and stains on concrete and plumbing fixtures, further indicating iron contamination (Plate 1) (bin Jusoh *et al.,* 2005; Carretero & Kruse, 2015; Elwakeel *et al.,* 2015).

Elevated iron levels in groundwater can lead to severe aesthetic and operational problems, including staining of infrastructure, dishes, clothes, plumbing fixtures and clogging infrastructure such as pipes and pumps (Hossain *et al*., 2015; Ishaque & Ritu, 2016). Long-term consumption of iron-rich groundwater can lead to iron overload disorders or hemochromatosis (with body iron levels ≥ 5 g) (Kew, 2014), which may cause organ damage particularly liver, kidney failure, neurological damage, vomiting, bleeding, and circulatory disorders (Ishaque & Ritu, 2016; Un-ei *et al*., 2006; Usman *et al*., 2021).

Although various techniques exist to address iron removal from groundwater, such as ion exchange, they are often impractical for rural households due to the need for high specialized techniques and chemicals. However, Africa boasts a rich diversity of plant species known for their medicinal and water-cleansing properties. Thus, the objective of this study was to assess the potential of baobab seeds-derived biochar in removing iron from groundwater, offering a feasible and affordable solution to improve access to clean and safe drinking water in Mpanda district, Tanzania.

Plate 1: **(A) A borehole that has been abandoned because of water metallic taste and (B) an example of a typical discolouration caused by Fe-contaminated groundwater to the concrete tank raiser found in the study area (Source: Mkelemi field survey, 2022)**

1.3   Rationale for the Study

Currently, there is increasing demand on the use of groundwater due to insufficient surface water to meet the rapidly growing population and increasing agricultural and industrial activities. This insufficiency stems from deteriorated surface water resources, over abstraction, and extended dry spells due to climate change. The present study was initiated to find the extent of contamination of groundwater with metallic species and to compare these levels with the existing WHO and TBS standards. This study also aimed at finding an affordable and readily available technique for iron removal in groundwater by assessing the effectiveness of baobab seeds-derived biochar. The significance lies in the uses of baobab seeds, their availability within the local area, and their affordability in the market for rural people.

1.4 The objectives of the Study

1.4.1 General Objective

The general objective of this study was to assess the extent of groundwater contamination and measure the effectiveness of the baobab seeds-derived biochar as a cost-effective Fe removal agent from groundwater.

1.4.2 Specific Objectives

The study focused on the two specific objectives:

(i)   To investigate the physicochemical characteristics and heavy metal concentrations of groundwater in Mpanda District, Tanzania.

(ii)   To assess the effectiveness of baobab seeds-derived biochar for removal of iron from groundwater.

1.5 Research Questions

This study sought to answer the following questions:

(i)   What are the physicochemical properties and heavy metals status of groundwater in the study area?

(ii)   What is the effectiveness of baobab seeds-derived biochar to remediate Fe ions from groundwater?

1.6 Significance of the Study

The findings from this study can be used by the Tanzania's Rural Water Supply and Sanitation Agency (RUWASA) to target specific aquatic pollutants and device efficient, cost-effective and decentralized mechanisms for improving the water quality in the disconnected remote areas of the country. The significance of the research study lies in its potential to address a critical issue affecting the livelihoods and health of communities in Mpanda district, Tanzania. By investigating the use of baobab seeds for clarifying groundwater contaminated with excessive iron, the study offers a promising solution that is both practical and affordable for rural households.

The research contributes to the body of knowledge by exploring a novel and sustainable approach to water treatment. Many existing technologies for iron removal from water often require advanced expertise and resources, rendering them inaccessible to many rural communities. By focusing on baobab seeds, which are locally available and known for their medicinal properties, the study introduces a culturally relevant and environmentally friendly solution.

Additionally, the research has practical implications for public health. Access to clean and safe drinking water is essential for preventing waterborne diseases and promoting overall well-being. By mitigating the adverse effects of iron contamination, the study has the potential to improve the quality of life for residents in Mpanda district.

Moreover, the research contributes to Sustainable Development Goal 6 by addressing water security and environmental conservation. By utilizing natural materials like baobab seeds for water treatment, the study aligns with principles of sustainability and resource efficiency.

1.7 Delineation of the Study

The study aimed to assess groundwater contamination in Mpanda District, Tanzania, and to evaluate the effectiveness of baobab seeds-derived biochar for iron removal. Groundwater samples from 19 boreholes in Mpanda district were assessed in rainy and dry season in February and in June 2023. The dual-season sampling approach allowed for a comprehensive analysis of seasonal variations in groundwater quality. Physicochemical parameters and heavy metals analyzed such as iron, manganese, lead, mercury and arsenic were assessed. Additionally, the study evaluated the effectiveness of biochar derived from baobab seeds in removing iron from the groundwater. However, the study focused specifically on iron removal and did not address the removal of other contaminants or biochar from different sources.

CHAPTER TWO

LITERATURE REVIEW

2.1 Introduction

This chapter provides a comprehensive perspective on Fe contamination in groundwater, addressing a fundamental aspect of public health. It begins by presenting an overview of groundwater quality, the status of Fe in groundwater, discussing treatment methods for Fe removal, and reviewing relevant theory and literature specific to the study topic. Additionally, it discusses how in recent years, biochar, a carbon-rich material produced from biomass pyrolysis, has emerged as a potential solution due to its adsorption properties.

2.2 Groundwater Quality

Groundwater quality serves as a pivotal indicator of water suitability for various purposes, ranging from drinking to agricultural and industrial applications (Wu *et al.*, 2020). It encompasses multiple dimensions crucial for assessing its usability and ecological impact. Firstly, it denotes the potability of groundwater, indicating whether it meets safety standards for human consumption without posing health risks (WHO, 2011). Additionally, the chemical composition of groundwater, including mineral content, salts, and pollutants, offers insights into its overall quality and potential contamination sources (El Azher *et al.*, 2008). Complementary to chemical aspects are physical characteristics such as temperature, turbidity, and odour, which influence water aesthetics and usability. Furthermore, groundwater quality has profound implications for ecological health, affecting aquatic ecosystems and biodiversity (Boulton, 2000; Danielopol *et al.*, 2003; Wang *et al.*, 2018). Sustainable groundwater management hinges upon maintaining water quality to support natural ecosystems while meeting human needs. Ultimately, ensuring access to clean and safe groundwater is paramount for safeguarding public health, promoting socio-economic development, and preserving water resources for future generations.

Groundwater quality is a significant concern for public health and environmental sustainability, and therefore several established organizations, including the World Health Organization (WHO), play key roles in setting standards and guidelines for controlling and managing groundwater quality. Overall, WHO and other organizations collaborate to establish and enforce standards, monitor groundwater quality, conduct research, and provide guidance on

best practices for managing and protecting this vital resource. Their efforts aim to ensure that groundwater remains safe and sustainable for drinking water supply and other uses while minimizing risks to human health and the environment. The World Health Organization (WHO) recommends a concentration of 0.3 mg/L for total Fe content in drinking water based on taste and colour considerations (WHO, 2011).

2.3 Iron Contamination in Groundwater

Iron (Fe), with atomic number 26 and symbol Fe, is one of the most abundant elements on Earth, constituting much of the planet's outer and inner core (Liu *et al.,* 2023). It ranks fourth in abundance after oxygen, silicon, and aluminum, with an atomic weight of 55.8 (Al-Fartusie & Mohssan, 2017). Naturally occurring, it is commonly found in deeper wells with minimal oxygen (El Azher *et al.,* 2008; Liu *et al.,* 2023).

2.3.1 Sources of Iron

(i) Natural Sources

Iron contamination predominantly stems from geological sources, where naturally occurring iron minerals dissolve into aquifers under specific geochemical conditions (Wang *et al.,* 2013). This dissolution occurs through weathering and the breakdown of iron-bearing minerals like iron oxides, hydroxides, and sulfides (Zhai *et al.,* 2021). The prevalence of contamination varies geographically, with regions characterized by iron-rich sedimentary rocks or aquifers with low oxygen levels, being more susceptible (Zhai *et al.,* 2021).

The form and solubility of Fe in water depend on factors like pH and the oxidation-reduction potential (Khatri *et al.,* 2017). Fe in water originates from minerals in igneous rocks, predominantly existing in the ferrous oxidation state (Fe^{2+}) (Khatri *et al.,* 2017). Under reducing conditions, minerals like pyrite (Fe_2S_2), marcasite (Fe_2S_2), and siderite ($FeCO_{3)}$ may precipitate, while under oxidizing conditions, sedimentary species such as ferric oxides (Fe_2O_3) or oxyhydroxides ($FeO(OH)$), like hematite (mineral composed of Fe_2O_3) and goethite (mineral composed of $FeO(OH)$), precipitate (Zhai *et al.,* 2021). These precipitates often have an underdeveloped crystalline structure and are commonly referred to as ferric hydroxides ($Fe(OH)3$) (Khatri *et al.,* 2017). Fe occasionally takes the form of siderite (mineral composed of $FeCO_3$), which is commonly present within layers of sandstone, mudstone, and limestone (Wu *et al.,* 2020).

(ii)   Anthropogenic Sources

While iron (Fe) in groundwater is primarily originates from natural sources, anthropogenic activities are also contributing to its availability (Palmucci *et al.,* 2016; Zhai *et al.,* 2021). These human interventions, including mining, industrial operations, and agriculture, introduce iron-containing compounds like ferric chloride and ferrous sulfate into the environment, exacerbating groundwater contamination (Jailos *et al.,* 2021; Latif *et al.,* 2020). Such activities not only directly pollute groundwater but also alter its environmental conditions, such as acid-base properties, redox conditions, pH, and microbial composition *(*Reta *et al.,* 2019; Zhai *et al.,* 2021). Moreover, organic matter particularly from anthropogenic sources, further complicates the hydrogeochemical processes, with higher concentrations of organics correlating with elevated Fe levels in groundwater (Wu *et al.,* 2020; Zhai *et al.,* 2021; Zhang *et al.,* 2019).

(iii)   Indicators of Iron Contamination in Mpanda's Groundwater

No prior research has evaluated groundwater quality in Mpanda, Tanzania, leaving a gap in understanding the region's water safety. An unpublished report from the Rural Water Supply and Sanitation Agency (RUWASA) indicates high concentrations of iron in groundwater samples from various locations within Mpanda. This finding is supported by observed colour, taste, and odour characteristics of the water, which suggest significant iron contamination (Hossain *et al.,* 2015). According to Hossain *et al.* (2015), pure water should be colourless, odourless, clear, and pleasant in taste. However, in Mpanda, groundwater stored in tanks and buckets exhibits a reddish-brown colouur, and similar discolouration is evident on concrete surfaces and plumbing fixtures (Mkelemi field survey, 2022). Additionally, the water has a metallic taste and an unpleasant odour, further corroborating the presence of iron contamination (Carretero & Kruse, 2015; Elwakeel *et al.,* 2015). These indicators underscored the urgent need to assess groundwater quality in Mpanda to address potential health risks and improve water management practices in the district.

2.3.2   Health and Environmental Impacts

Fe is an essential nutrient crucial for various bodily functions, including oxygen transport, energy production, and DNA synthesis (Fraga, 2005). It plays a vital role in metabolic processes like oxygen and electron transport and the synthesis of DNA (Fraga, 2005; Kostrzewa, 2014). Iron is also necessary for growth, development, normal cellular functioning,

and the synthesis of certain hormones and connective tissue (Al-Fartusie & Mohssan, 2017; Fraga, 2005). However, excessive long-term consumption of Fe in water can have detrimental effects on both human health and the environment. The World Health Organization (WHO) recommends that the iron concentration in drinking water should not exceed 0.3 mg/L to avoid taste and colour issues. High Fe concentrations can cause aesthetic issues like a metallic taste, staining of plumbing fixtures, and water discolouration (Rushdi *et al.,* 2023; Wang *et al.,* 2013). Furthermore, long-term consumption of iron-rich groundwater (with body iron levels ≥ 5 g) (Kew, 2014), can lead to iron overload disorders, such as hemochromatosis, which can cause neurological disorders like Alzheimer's and Parkinson's diseases, cardiovascular issues, and respiratory disorders (Kostrzewa, 2014; Salvador *et al.,* 2011; Schröder *et al.,* 2013).

2.4   Iron Removal Methods

Various iron treatment methods to remove iron from groundwater have been reviewed including conventional methods, biological methods, membrane technology-based strategy, and nanotechnology-based strategy. Additionally, an emerging method using plant extracts has been reviewed for iron removal from groundwater.

2.4.1   Conventional Methods

(i)   Chemical Oxidation

Chemical oxidation is a water treatment process used to convert dissolved contaminants, such as ferrous iron (Fe^{2+}), into insoluble forms that can be easily removed from the water. This method involves chemical oxidants such as chlorine, potassium permanganate, or hydrogen peroxide of which can be added to groundwater to facilitate the oxidation of ferrous iron to ferric iron (Isaeva & Castro, 2011). Coagulation, flocculation, sedimentation, and filtration are the main steps in the chemical purification process. Iron can be removed by clarity utilizing coagulation and sedimentation processes when present in very high concentrations or in situations where a rapid reaction is desired (Hashim *et al*., 2011; Mcpeak & Aronovitch, 1983). As a result, chemical coagulants are the most efficient water treatment techniques, but they also have serious negative consequences on the environment and public health. Chemical coagulants, however, have a number of drawbacks, including the fact that they are extremely poisonous, non-degradable, expensive, corrosive, and impractical to employ (Pascu *et al*., 2016). They are also scarce and modify the pH, acidity, hardness, and other properties of treated

water, which can lead to serious health problems like cancer and neurological illnesses like Alzheimer's disease (Mutula Joseph, 2016).

(ii)   Aeration and Oxidation

Aeration and oxidation method is a common technique used to remove iron from groundwater by promoting the conversion of soluble ferrous iron (Fe^{2+}) to insoluble ferric iron (Fe^{3+}), which can then be filtered out. Aeration and oxidation are the two incorporated steps in the purification process followed by filtration process.

Aeration

Aeration involves exposing groundwater to air or oxygen to promote the oxidation of ferrous iron to ferric iron. This process can occur naturally through the movement of water in contact with air, or it can be facilitated using mechanical aeration system. Mechanical aeration systems typically use aerators, diffusers, or cascading water systems to maximize the surface area of contact between the water and air, enhancing the oxidation process. As the groundwater is aerated, dissolved oxygen from the air reacts with ferrous iron, initiating the oxidation reaction.

Oxidation

The oxidation reaction involves the conversion of ferrous iron (Fe^{2+}) to ferric iron (Fe^{3+}), which forms insoluble ferric hydroxide precipitates. The overall reaction can be represented as follows: $4Fe^{2+} + O_2 + 4H_2O \rightarrow 4Fe(OH)_3$ (1)

This reaction occurs rapidly in the presence of dissolved oxygen and can also be catalyzed by other oxidizing agents such as chlorine or potassium permanganate.

The process requires adequate retention time to ensure sufficient contact between the groundwater and the oxidizing agent or air to complete the oxidation reaction. The duration of aeration and oxidation may vary depending on factors such as the concentration of iron, the flow rate of groundwater, and the design of the aeration system.

Filtration

Following the oxidation process, the water is directed to filtration units, typically consisting of sand or multimedia filters, to remove the insoluble ferric hydroxide precipitates. Filtration

removes the precipitated iron particles, as well as any other suspended solids, turbidity, or impurities present in the water, resulting in clarified water.

Generally, the aeration and oxidation method require expertise to monitor and control. Throughout the aeration and oxidation process, water quality parameters such as dissolved oxygen levels, pH, iron concentration, and turbidity are monitored to assess treatment performance and optimize operating conditions. Control systems may be employed to regulate aeration rates, oxidant dosage, pH levels, and other process parameters to ensure effective iron removal and compliance with regulatory standards (Haouti *et al.*, 2018).

(iii)   Polyphosphates

Polyphosphates can be used to remove the iron during treatment by surround iron, keeping or trapping it so that it become unavailable (Chandler, 1989; Scherer, 2019). This treatment must be applied to the water before it is exposed to air or before chlorination in order for polyphosphate to be used effectively (Scherer, 2019). However, the polyphosphates do not remove iron from water; instead, they sequester it, keeping it in solution. Therefore, while polyphosphates can help prevent iron-related issues such as staining and scaling, they do not address the underlying cause of iron contamination and may not be suitable for all water treatment scenarios, particularly those with high iron concentrations (Mutula, 2016).

(iv)   The Greensand

The glauconite in the greensand is extracted, cleaned, screened, and subjected to chemical treatments to create a long-lasting, greenish-black product having the capacity to adsorb soluble iron and manganese (Michel *et al.,* 2020; Pepper, 1980). Metals can be successfully removed from water using glauconite after it has undergone chemical regeneration, but raw glauconite also demonstrates exchange capacity (Michel *et al.,* 2020). After being stabilized, the glauconite is covered in manganese oxide. Because of its coating, glauconite has unique chemical oxidation-reduction abilities to remove iron, manganese, and trace amounts of hydrogen sulfide (Qin *et al.,* 2009). But this method is expensive as it needs expertise and chemicals such chlorine, soda ash, and calcium hypochlorite (Rader, 2009).

(v)   Removal by Ion Exchange

Ion exchange involves passing groundwater through resin beds containing exchangeable ions, such as zeolites or synthetic resins, which selectively adsorb dissolved iron ions. In this approach, hydrogen peroxide (H_2O_2) and an iron ion source are used as Fenton's reagents in the processes. The strong hydroxyl radical (HO) production and change in the oxidation state of Fe^{2+} to Fe^{3+} are the causes of the method's high efficiency (Mutula, 2016). The fundamental problem with Fenton's method is the development of ferric sludge. Ion exchange (IE) serves as a complement to the Fenton process in this study, enabling, on the one hand, the removal of the excess iron contained in the sludge. Iron may also be removed by ions. The resins in the softener will remove the iron ions from the water if it hasn't been exposed to oxygen. Iron deposits may accumulate on the resin if the water has any dissolved oxygen. The resin can be cleaned, but doing so costs money, and each washing results in less resin being able to hold its shape (Pascu *et al.,* 2016). This method is effective for removing both ferrous and ferric iron ions from groundwater and can be regenerated for reuse by flushing with a regenerant solution.

2.4.2   Biological Methods

The biological method for removing iron from water uses natural processes involving microorganisms, such as iron-oxidizing bacteria (e.g., *Leptothrix sp.*, *Flavobacterium sp.*, *Gallionella sp.*, *Sphaerotilus sp.*, and *Siderocapsa sp.*). These bacteria oxidize soluble ferrous iron (Fe^{2+}) into insoluble ferric iron (Fe^{3+}), which then forms iron oxides or hydroxides that precipitate out of the water. This process allows for the removal of iron through sedimentation and filtration, making it an effective and environmentally friendly approach (Khatri *et al.,* 2017).

The biological method of iron removal from water, though effective and environmentally friendly, has several drawbacks. One major challenge is the time-consuming nature of the process. Biological iron removal relies on the growth of microorganisms and the natural oxidation of iron, which often takes longer than chemical methods. This extended timeframe can be problematic in situations where rapid iron removal is needed (Khatri *et al.,* 2017).

2.4.3   Membrane Technology-Based Strategy

Membrane technology-based strategies for iron removal from water involve using specialized membranes to separate and remove iron ions from contaminated water. Membrane filtration involves passing water through a semi-permeable membrane that allows clean water to pass through while retaining contaminants, including iron ions (Bora & Dutta, 2019; Khatri *et al.,* 2017). Various types of membranes can be used depending on the size and type of contaminants including reverse osmosis (RO), microfiltration (MF) and ultrafiltration (UF) (Le & Nunes, 2016). Each type has different pore sizes and filtration capabilities.

Membrane technology can be expensive to install and maintain (Khatri *et al.,* 2017). The initial capital cost for membrane systems and the cost of replacing membranes periodically can be high (Khatri *et al*., 2017). Even though membrane technology is a straightforward process, the entire system is complex.

2.4.4   Nanotechnology-Based Strategy

Nanotechnology-based strategies for iron removal from water leverage the unique properties of nanoscale materials to target and eliminate iron ions effectively. These strategies typically involve the use of advanced nanomaterials, such as metal oxide nanoparticles (e.g., iron oxide or titanium dioxide) and carbon-based nanomaterials (e.g., carbon nanotubes or graphene), which have extremely high surface areas (Khatri *et al.,* 2017). This high surface area provides numerous active sites for iron ions to attach, making the process of adsorption highly efficient. Additionally, nano-filtration membranes, designed at the nanoscale, can selectively filter out iron particles, allowing clean water to pass through while retaining contaminants. Nanomaterials can remove iron ions with great precision, often achieving near-complete removal.

However, the application of nanotechnology in iron removal is not without its drawbacks. The cost of producing and applying nanomaterials can be prohibitively high, particularly for large-scale or budget-constrained projects (Khatri *et al.,* 2017). This expense stems from the high cost of raw materials and the need for advanced manufacturing techniques.

2.4.5 Challenges

Despite advancements in iron removal technologies, challenges remain in treating groundwater contaminated with iron, particularly in rural or resource-constrained areas. Factors such as high iron concentrations, fluctuating water chemistry, and limited access to treatment infrastructure pose significant challenges to ensuring safe drinking water for affected communities. This study focused on developing cost-effective, sustainable, and scalable treatment solutions tailored to the specific needs of regions affected by iron contamination in groundwater.

In recent years, the exploration of biochar as a sustainable and efficient medium for water treatment has gained considerable attention (Bayuo *et al.,* 2023b). Among the diverse feedstocks used to produce biochar, baobab seeds have emerged as a promising candidate due to their abundance in certain regions particularly to arid and semi-arid climate regions and unique chemical composition (Edogbanya *et al.,* 2016; Gebauer *et al.,* 2016). This study delves into the application of baobab seeds-derived biochar for the removal of iron from groundwater. By harnessing the unique properties of baobab seeds-derived biochar, the study aimed to address the pervasive issue of iron contamination in groundwater sources. This exploration involves an examination of how the properties of baobab seeds biochar are optimized to effectively sequester iron ions and enhance water quality.

2.5   Properties, Water Treatment Applications, and Kinetic Models of Biochar

2.5.1   Properties of Biochar

Biochar, a carbonaceous material produced through the pyrolysis of organic biomass under oxygen-limited conditions, has gathered significant interest in various fields, including agriculture, environmental remediation, and water treatment (Priyadarshni *et al*., 2020). Its unique properties make it an attractive option for mitigating environmental challenges, particularly in the realm of water purification (Xinyu, 2023). Conventional iron removal methods, such as chemical oxidation and filtration, have drawbacks including high costs and environmental impact. Plant-based materials offer a promising alternative due to their abundance, low cost, and eco-friendly properties (Priyadarshni *et al*., 2020; Rwiza *et al*., 2020). For instance, biochar and activated carbon possess unique physical and chemical properties that make them suitable for water purification (Rwiza *et al*., 2018). Both materials exhibit high surface area, porous structure, and strong adsorption capacity, enabling efficient removal of

iron ions from water through physical and chemical interactions (Patra *et al*., 2017; Rwiza *et al*., 2018).

Physical Structure

Biochar exhibits a highly porous structure, characterized by a network of interconnected pores spanning a range of sizes, from micro to macro. This porous morphology provides an extensive surface area for the adsorption and retention of contaminants

Chemical Composition

The chemical composition of biochar varies depending on the feedstock used for its production and the pyrolysis conditions employed. While primarily composed of carbon, biochar may also contain small amounts of elements such as hydrogen, oxygen, nitrogen, and mineral residues derived from the parent biomass. Functional groups, including hydroxyl (-OH), carboxyl (-COOH), and phenolic (-Ph) groups, contribute to biochar's surface chemistry and its interaction with contaminants.

Surface Area and Porosity

The surface area and pore structure of biochar play a crucial role in its adsorption capacity and efficiency. High surface area, coupled with a diverse pore size distribution encompassing micropores, mesopores, and macropores, enables biochar to effectively adsorb a wide range of contaminants from aqueous solutions due to availability of ample sites for the adsorption of contaminants. The surface area and pore size distribution of biochar influence its adsorption capacity and kinetics, with greater surface area and pore volume generally corresponding to higher adsorption efficiency.

Adsorption Properties

Biochar exhibits a strong affinity for a wide range of contaminants, including heavy metals, organic pollutants, and pathogens, through physical and chemical mechanisms. Physical adsorption occurs via van der Waals forces and pore filling, while chemical adsorption involves processes such as ion exchange, complexation, and surface precipitation. The adsorption capacity of biochar for specific contaminants depends on factors such as the chemical nature of the contaminant, solution pH, temperature, and the presence of competing ions.

2.5.2 Kinetic Models for Adsorption

The mechanism of adsorption and its potential rate-controlling steps, including mass transport and chemical reaction processes, are often investigated using kinetic models. Kinetic studies involve batch reactions with varying initial sorbate concentrations, sorbent doses, particle sizes, agitation speeds, pH values, and temperatures to determine the rate of solute removal, controlling the residence time of the sorbate in the solid–solution interface. Linear regression is commonly used to determine the best-fitting kinetic rate equation. Among the various kinetic models, the pseudo-first and pseudo-second-order rate models are commonly used in biosorption studies.

(i) Pseudo-First-Order Kinetic Model

The Pseudo-first-order kinetic model is widely used in adsorption studies to describe the rate at which a substance adsorbs onto a solid surface, such as activated carbon or biochar (Vunain *et al*., 2017). It assumes that the rate of adsorption is directly proportional to the difference between the equilibrium adsorption capacity q_e and the amount of substance adsorbed at a given time q_t (Vunain *et al*., 2017). While this model offers simplicity and ease of application, it may not always accurately represent adsorption kinetics due to factors like surface heterogeneity and mass transfer limitations. Mathematically, the model is expressed as equation (2) (Rao *et al*., 2010):

$$\frac{dq_e}{dt} = k_1 \left(q_e - q_t\right) \tag{2}$$

where q_e (mg/g) represents the amount adsorbate (iron) adsorbed at equilibrium, while q_t (mg/g) denotes the amount adsorbate (iron) adsorbed at time t (min). The rate constant for the Pseudo-first order reaction is denoted as k_1 (per min) (Rao *et al*., 2010).

(ii) Pseudo-Second-Order Kinetic Model

The Pseudo-second-order kinetic model is employed to study adsorption processes, particularly in wastewater treatment. It posits that the rate of adsorption is proportional to the square of the difference between the equilibrium adsorption capacity q_e and the amount of substance adsorbed at a given time q_t (Vunain *et al*., 2017). This model accounts for more complex adsorption mechanisms, including surface interactions and chemical bonding, making it suitable for systems influenced by factors like diffusion processes (Vunain *et al*., 2017).

However, deviations from this model may occur under non-ideal conditions, such as heterogeneous surfaces or competitive adsorption. Mathematically, it is expressed as equation (3) (Rao *et al*., 2010).

$$\frac{dq_t}{dt} = k_2 \, (q_e \, - q_t)^2 \tag{3}$$

Where $\frac{dq_t}{dt}$ signifies the rate of adsorption at time t, K_2 denotes the rate constant of the Pseudo-second-order kinetic model, q_e stands for the equilibrium adsorption capacity and q_t represents the amount of substance adsorbed at time t (Rao *et al*., 2010).

2.5.3   Adsorption Mechanisms

Adsorption is a purification process employing an adsorbent like biochar and or activated carbon to eliminate organic contaminants, unwanted colours, and taste- and odour-causing compounds from water (Al-Ghouti & Da'ana, 2020). These pollutants adhere to the surface of biochar or activated carbon, thus being extracted from the drinking water (Patra *et al*., 2017). The adsorption mechanisms involve physical adsorption, where iron ions attach to the material's surface, and chemical adsorption, including ion exchange and complexation reactions (Patra *et al*., 2017). These mechanisms enable the retention of iron ions within the porous structure of the adsorbents, resulting in efficient removal from water solutions (Al-Ghouti & Da'ana, 2020).

Despite recent studies investigating the adsorption properties of plant-based materials for metal ion removal from groundwater, there remain significant challenges and knowledge gaps. Notably, the study by Edogbanya *et al*. (2016) highlights potential limitations of using baobab seeds powder for water treatment. The organic content of baobab seeds may cause contamination during transportation or storage, posing a risk to water safety. This underscores the need for further research to converting baobab seeds powder into biochar.

To address the gap, this study focused on developing sustainable and effective solutions for iron removal from groundwater using baobab seeds-derived biochar. By investigating the carbonization process and evaluating the adsorption capabilities of baobab-derived biochar, this research aimed to contribute valuable insights and practical applications for water treatment technologies.

CHAPTER THREE

MATERIALS AND METHODS

This chapter describes the materials and methods used to achieve the objectives. It also gives an overview of the study area.

3.1   Study Area

Mpanda is a District which is the headquarters of the Katavi region (Fig. 1a and 1b). Mpanda district is a staging point for visiting the Katavi National Park, with its about 35 km to the south of Sitalike. As per the 2022 census report, Mpanda District which is the headquarters of the Katavi region, have 446,866 residents (Knowles & Wareing, 2022). Mpanda is 1085 m above sea level and is situated at latitude 6° 20' 52.0" S, and longitude 31° 4' 25.1" E. The district has a unimodal rainy season from November to April and a dry season from May to October. The climate is favourable with an average maximum temperature of 27°C. The district receives around 1000 mm to 1500 mm of rainfall per year.
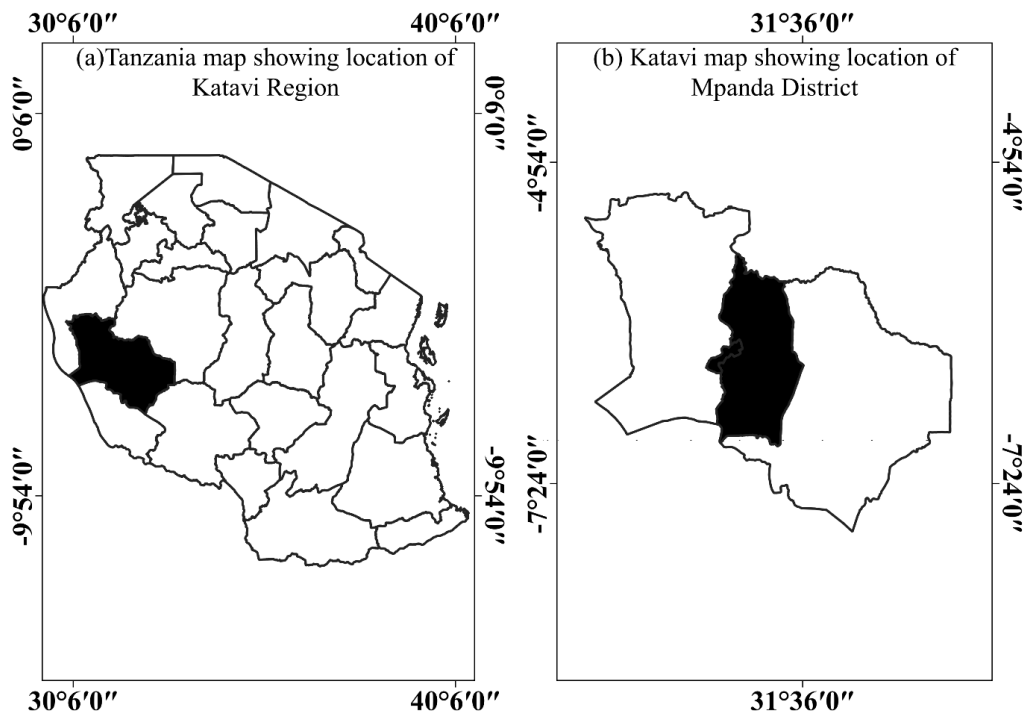
Figure 1:   **Map of Tanzania showing the location of Katavi region (a); and a map of Katavi region showing the location of Mpanda district (b)**

3.2   Study Design

In Mpanda district, 19 boreholes (Fig. 2) were randomly selected for groundwater sample collection and their precise locations were recorded using handled global positioning system (Garmin Etrex 10). The 19 sampled boreholes were located in 19 villages, namely Ilembo (B01) Kashaulili (B02), Mtisi (B03), Sugar (B04), Kamakuka (B05), Itenka A (B06), Society (B07), Magula (B08), Kapanda (B09), Kampuni (B10), Magamba (B11), Dirifu (B12), Ibindi (B13), Katisunga (B14), Kasimba (B15), Mapinduzi (B16), Kapalala (B17), Makanyagio (B18) and Majengo (B19). Most of the sampled boreholes were the main source of water for domestic use in the study area.
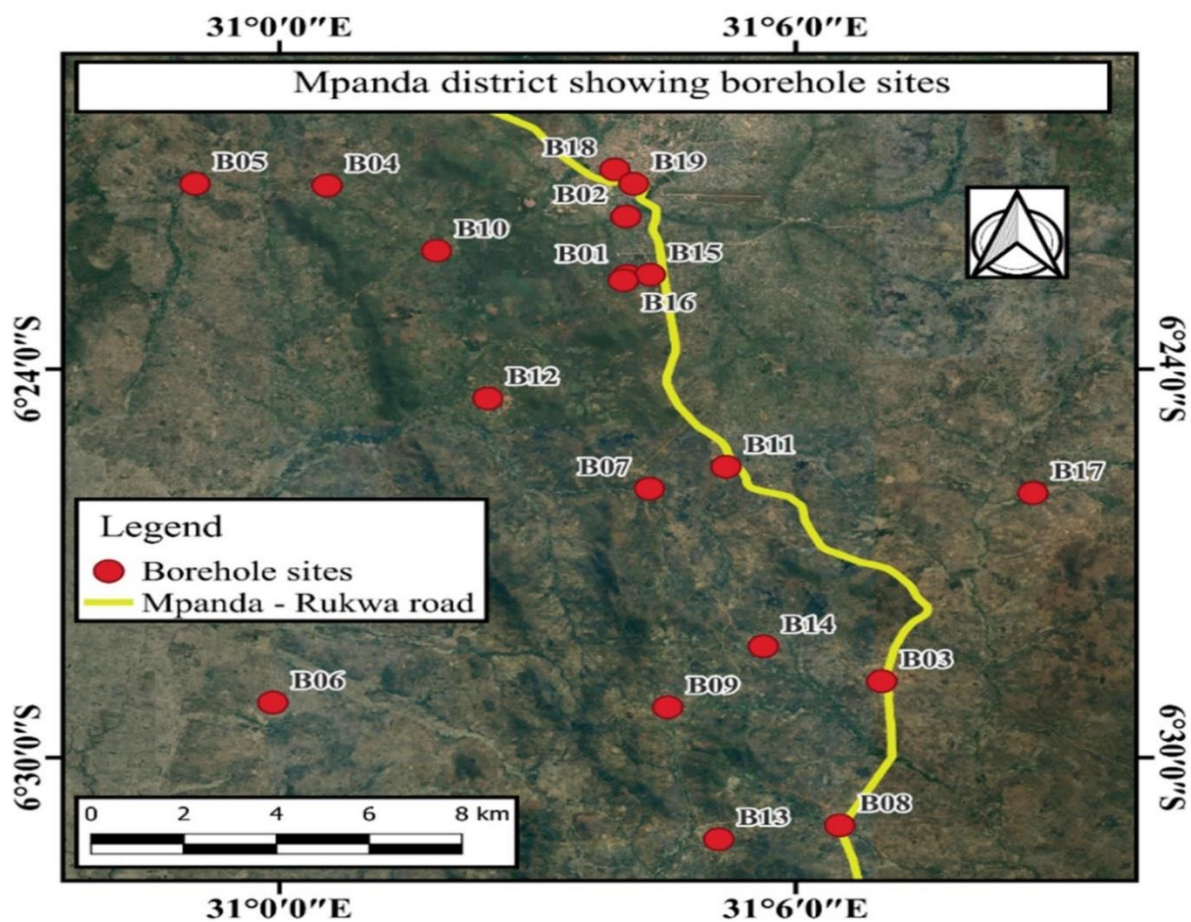
Figure 2:   Map of the Mpanda district showing the location of 19 sampled boreholes

3.3   Groundwater Quality Assessment in Mpanda District, Tanzania

3.3.1   Water Sampling and Preservation

Groundwater samples were taken from hand and electric pump-equipped boreholes for the evaluation of physicochemical properties and heavy metal concentrations in groundwater.

These samples were collected in February and June 2023, representing the rainy and dry seasons respectively.

Samples were collected in triplicate making a total of 114 samples for analysis (APHA, 2012). Water samples for physicochemical analysis were collected in a 1 L of high-density polyethylene (HDPE) plastic bottle. The bottles were prior carefully cleaned and rinsed with distilled water, and then three times washed with sample water before sampling. Samples were acidified with 10% HNO_3 to pH ≤ 2 to maintain heavy metals in the solution and prevent them adherence to container surfaces (Adongo *et al*., 2022). Water samples were collected after allowing the water to flow out for about five minutes after pumping. This measure was adopted to guarantee that the collected water truly reflected the genuine state of the borehole (APHA, 2012). Samples were stored and transported in lightproof cooling box contained ice packs to the Nelson Mandela African Institution of Science and Technology (NM-AIST) laboratory and Arusha Technical College laboratory within 48 hours for analyses. In the laboratory, samples were refrigerated at 4°C before analysis. The entire process adhered to established procedures following APHA and WHO protocols, ensuring consistent and high-quality data.

3.3.2 Physicochemical Parameters and Heavy Metals Assessment

Various physicochemical parameters were analyzed both in situ and in the laboratory. At the collection point, parameters including temperature (°C), pH, electrical conductivity (EC) (µS/cm), total dissolved solids (TDS) (ppm), and dissolved oxygen (DO) (mg/L) were assessed using a Hach multiparameter (model 40HQd) (Plate 2 A). Turbidity (NTU)) was measured using a turbidimeter (Germany's AL 250 L). Hardness (mg/L) was determined using the EDTA titrimetric method. Chloride levels (mg/L) were determined using argentometric titration with silver nitrate. Heavy metal concentrations including manganese (Mn) (mg/L), lead (Pb) (µg/L), mercury (Hg) (µg/L) and arsenic (As) (µg/L) were determined using the Atomic Absorption Spectrophotometer (AAS) method (Plate 2 B) following established APHA protocols (APHA, 2012). Hach spectrophotometer DR6000, employing FerroVer iron reagent and distilled water for calibration, was used to measure iron (Fe) (mg/L) concentration (Plate 2 C).

Plate 2:   **Instruments used in measuring the physicochemical water quality parameters and analysis of the heavy metal concentrations. A – Multiparameter (40HQd), B – Atomic Absorption Spectrophotometer (AAS), C – Hach spectrophotometer (DR6000)**

3.3.3 Water Quality Index (WQI)

Water Quality Index (WQI) for human consumption was examined for the groundwater samples to get a comprehensive summary of quality status and level of pollution (Ukah *et al*., 2019). The WQI was computed using the weighted arithmetic method for water-quality index assessment (Rahman *et al*., 2018). Three steps were taken in evaluating the WQI for each of the samples. Initially, weights were allocated to the physicochemical parameters and heavy metals, considering the significance of each parameter in the overall water quality for drinking and domestic uses (Akhtar *et al*., 2014; Jha *et al*., 2020; Ukah *et al*., 2019). With the assigned weights, the relative weight of each parameter was calculated using the formula equation (4).

$$W_i = \frac{w_i}{\sum_i^n w_i} \qquad\qquad (4)$$

where W_i is relative weight, w_i is weight of parameter, and n is the total number of parameters. The assigned weights and the calculated relative weights for the 13 analyzed parameters are depicted in Table 6. Secondly, the quality rating scale for each of the parameters was calculated. This was done by dividing each parameter's concentration in the water samples by the respective standard value and multiplying the results by 100 equation (5).

$$q_i = \frac{C_i}{S_i} \times 100 \qquad\qquad (5)$$

where q_i is quality rating, C_i is the concentration of each parameter, and S_i is the standard value for the parameter. The last step of the GWQI was the determination of sub-index for each parameter and then the summation of all sub-indices for each sample, as shown in Equations 6 and 7, respectively.

$$SI_i = W_i \times q_i \qquad\qquad (6)$$

$$GWQI = \sum_i^n SI_{i-n} \qquad\qquad (7)$$

where SI_i is the sub-index of ith parameter, q_i is the quality rating with respect to concentration of ith parameter and n is the number of parameters (Mgbenu & Egbueri, 2019). WHO (WHO, 2011) and TBS (TBS, 2018) standard values were used in this indexing.

23

3.3.4 Data Analyses

Data were organized and summarized in Microsoft Excel (Windows 10). The IBM SPSS Version 27.0 software, was used to perform data analyses. Descriptive statistics including minimum, maximum, mean, and standard error of the mean for physicochemical and heavy metal concentrations at each borehole were calculated for the rainy and dry seasons. Provided that most parameters did not meet the normal distribution criteria required for parametric tests (Shapiro Wilk-test, p-values ≤ 0.05), the non-parametric Wilcoxon signed rank test (Noether, 1992) at 95% confidence level was employed for testing significant differences in the physicochemical and heavy metal concentrations between seasons. Furthermore, the Kruskal-Wallis test was opted for comparisons across boreholes (Sheskin, 2020), the boreholes were grouped into four wards (Table 1). The Spearman correlations-rank test was applied to explore whether the physicochemical variables are associated with heavy metal concentrations. The study employed Principal Component Analysis (PCA) and Spearman's correlation test to explore the relationships between physicochemical parameters and heavy metals, assessing their variability. According to Taylor *et al.* (1990), correlations with Spearman's $r > 0.35$ indicate parameters are not independent, while values $r > 0.68$ suggest strong correlations among parameters. In case of strong correlation across scales, it is impossible to distinguish the physicochemical parameters and heavy metal concentrations.

Table 1:   Ward-based groups of boreholes in Mpanda District

Group 1 (Ilembo ward)		Group 2 (Magamba ward)		Group 3 (Sitalike ward)		Group 4 (Kakese ward)	
Borehole Code	Villages	Borehole Code	Villages	Borehole Code	Villages	Borehole Code	Villages
B01, B16, B15, B02, B18, B19	Ilembo, Mapinduzi, Kasimba, Kashaulili, Makanyagio, and Majengo	B07, B11, B12, B17	Society, Magamba, Dirifu, Kapalala	B03, B08, B09, B10, B13, B14	Mtisi, Magula, Kapanda, Kampuni, Ibindi, Katisunga	B04, B05, B06, B10	Sugar, Kamakuka, Itenka A, Kampuni

3.4   Potential Use of Baobab Seeds to Remove Iron from Groundwater

The experiment from this sub-section was conducted to assess the potential use of baobab seeds-derived biochar to adsorb iron from the groundwater.

3.4.1 Collection and Preparation of the Adsorbent (Baobab Seeds-Derived Biochar)

This study utilized biochar derived from baobab seeds *(Adansonia digitata L)* as an adsorbent to remove iron from groundwater. The baobab seeds, sourced locally in Mpanda market, underwent a rigorous cleaning process with distilled water to eliminate surface impurities. Subsequently, the seeds were sun-dried for 2 days and air-dried at 105 ℃ in a hot air oven and subjected to carbonation (pyrolysis) in a Gallonhop Muffle furnace at 700 ℃ temperature for 2.5 hours burning period, a thorough carbonation process, and complete furnace coverage that minimized air interference, with a controlled temperature increase of 8–10 ℃ min^{-1}. Following a 20 minutes residence time, the furnace was gradually cooled to 40–50 ℃. The resulting carbonized seeds were finely ground to fine powder using a blender, sieved through a 90 μm mesh, and stored in an airtight plastic container. The biochar preparation followed an approach by Tabassum *et al*. (2019).

3.4.2 Characterization of the Adsorbent Baobab Seeds-Derived Biochar

The morphological characteristics of the adsorbent, baobab seeds-derived biochar, were investigated using a ZEISIS SIGMA 300 VP scanning electron microscope (SEM) coupled with Smart EDX. To prevent charge accumulation during measurement, the samples were placed on double-sided carbon conductive tape and double-coated with a carbon layer using a Quorum Q150T ES instrument. Additionally, Shimadzu X-ray diffraction patterns for baobab seeds-derived biochar were obtained using a Pan-Analytical Goniometer with Cu Ka radiation source. The scanning range was 5–80 degrees over a 2 minutes period at 30 kV and 15 mA.

The textural properties of baobab seeds-derived biochar were determined through nitrogen sorption at -77 K after degassing the samples at 160 °C for 4 hours. The Quanta-chrome NOVA 1200e Series pore size and surface area analyzer were employed, with the specific surface area calculated using the Brunauer–Emmett–Teller (BET) method. The total pore volume (VT) was estimated based on the nitrogen adsorbed at a relative pressure of P/P0 * 0.99.

3.4.3 Collection of Groundwater Samples for Iron Removal Using Baobab Seeds-Derived Biochar Experiment

Groundwater sample was collected from the borehole at Ilembo village in Mpanda district using polyethylene containers at latitude 11°8′4.39″ Nand longitude 7°39′26.24″ E. The actual location of collection was determined using a handled Global Positioning System (GPS) unit.

The first 50 – 100 mL of sample was used to rinse the containers first before the required volume was collected. The initial iron of groundwater water was about 6.02 mg/L.

3.4.4 Adsorption Kinetics Experiments for Iron Removal

(i)   Effect of Doses of the Adsorbent

The study systematically explores the influence of varying doses of the adsorbent (baobab seeds-derived biochar) on the removal of iron from untreated field water. Adsorption kinetics experiments were conducted using a flocculator (PCI Ltd, England). Six 1000 mL water beakers were filled with groundwater, and adsorbent doses of 0.6 g, 1.2 g, 1.8 g, 2.4 g, and 3.0 g were added, with one water beaker serving as a control. A stirring machine ensured consistent mixing of water and adsorbent, involving 3 minutes of rapid mixing at 100 rpm followed by 17 minutes of slow mixing at 30 rpm. Subsequently, samples underwent filtration using Whatman paper No. 1 (11 µm), and the filtrate was analyzed using the DR6000 Spectrophotometer to determine residual iron concentrations. The entire experimental procedure was repeated thrice for reliability and reproducibility, and obtained values were computed to get the averages.

(ii)   Effect of Adsorption Temperature, Solution Ph, Adsorbent Particle Size, Contact Time

The study also investigated the impact of adsorption temperature, solution pH, adsorbent particle size, initial iron concentration, and contact time on iron removal in the adsorption kinetic test experiment. For the adsorption temperature study, experiments were conducted at temperatures ranging from 20 °C to 50 °C while keeping other parameters constant. The effect of solution pH on iron ion removal was investigated by adjusting the pH from 2.0 to 12.0 using 0.1 M hydrochloric acid (HCl) or 0.1 M sodium hydroxide (NaOH). Particle size analysis involved sieving the adsorbent through different sizes (90 µm to 1000 µm), maintaining a constant dose and other parameters. The same procedures were applied with the effect of contact time keeping the rest parameters constant with varying time intervals ranging from 15 minutes to 120 minutes.

(iii)   Effect of Initial Concentration

To examine how the initial concentration of iron affects the adsorption capacity, iron solutions with initial concentrations ranging from 2 mg/L to 50 mg/L were prepared using Fe_2SO_4. Adsorption experiments were conducted by adding a fixed amount of adsorbent to each iron solution while maintaining constant conditions for other variables, such as temperature, solution pH, adsorbent particle size, and contact time. After sufficient contact time for adsorption equilibrium, the solutions were filtered to separate the adsorbent, and the remaining iron concentration was measured using the DR6000 Spectrophotometer.

The iron removal efficiency (R_e) for each case was determined using Equation 8.

$$\% \, Re = \frac{C_o - C_t}{C_o} \times 100 \tag{8}$$

where % Re represents the removal efficiency C_o and C_t (mg/L) denote the initial and time t concentrations of iron, respectively.

With the synthesized iron-contaminated water being prepared, a series of iron solutions with varying initial concentrations (e.g., 1, 2, 3, 4, 5, 6 and 7 mg/L) were poured into 1000 ml beakers and a known quantity of baobab-seeds biochar (3 g) was added to each beaker. These beakers were agitated on a rotary shaker at a constant speed (i.e 120 rpm) and maintained at a temperature of 25 °C, with samples withdrawn at regular intervals of ranging from 15 to 180 minutes for analysis of residual iron concentration using a spectrophotometer DR 6000. The adsorption capacity of the biochar at equilibrium (q_e) was calculated using mass balance equation (9).

$$q_e = \frac{C_o - C_e \times V}{m} \quad in \, mg/g \tag{9}$$

where: q_e represents the adsorption capacity at equilibrium (in mg/g), C_o is the initial concentration of the solute in the solution (in mg/L), C_e is the equilibrium concentration of the solute in the solution (in mg/L), V is the volume of the solution (in L) and m is the mass of the adsorbent material used (in g).

3.4.5 Adsorption Modelling and Kinetics

(i) Adsorption Isotherm

The equilibrium data for synthesized biochar were analyzed using both Langmuir and Freundlich models, which are the mathematical frameworks considering factors such as adsorbent homogeneity/heterogeneity, interaction between species, and coverage type, in the adsorption process (Vunain *et al*., 2017). These isotherms offer insights into the system's behavior, adsorbent efficiency, and economic viability. The linear form of the Langmuir isotherm (described by Equation (10) was employed, and the corresponding plot of C_e/q_e (mg/g) against C_e (mg/L) was used to determine maximal adsorption capacity (q_m) and adsorption intensity (K_L) based on the slope and intercept of the line.

$$\frac{C_e}{q_e} = \frac{1}{q_m K_L} + \frac{1}{q_m} C_e \tag{10}$$

where, C_e represents the equilibrium concentration (measured in mg/L), q_m is the maximum adsorption capacity per unit weight of adsorbent (measured in mg/g), K_L is the Langmuir constant indicating the sorption energy between the adsorbate and adsorbent (measured in L/mg), and q_e denotes the adsorbent's monolayer adsorption capacity (measured in mg/g).

The derivation of the equilibrium coefficient, specifically the separation factor R_L, was crucial for determining the favorability of the adsorption process. Equation (11) was employed to achieve this goal. The separation factor R_L is a key parameter used to assess whether the adsorption process is favorable ($R_L < 1$), unfavorable ($R_L > 1$), or approaching irreversibility ($R_L = 1$) (Vunain *et al*., 2013).

$$R_L = \frac{1}{1 + q_m C_o} \tag{11}$$

where, C_o represents the highest initial concentration of metal (iron) in water (mg/L).

The expression of the Freundlich model is shown in equation (12).

$$Log q_e = Log K_F + (1/n) Log C_e \tag{12}$$

Here, C_e is the equilibrium concentration of the adsorbate (mg/L), q_e is the quantity of metal (Fe) ions adsorbed at equilibrium (mg/g), K_F is the Freundlich constant reflecting adsorption

capacity, and n is the Freundlich constant representing adsorption intensity. The intercept and slope of a plot showing $\log q_e$ vs $\log C_e$ were used to determine the values of K_F and n.

The K_F and n values related to the model, displays that, adsorption is favorable when n exceeds one. The slope $1/n$, ranging from 0 to 1, gauges adsorption intensity or surface heterogeneity; as it nears zero, the surface becomes more heterogeneous (Vunain *et al.*, 2013).

Both linearized models, Freundlich and Langmuir, demonstrate a satisfactory fit to the experimental data. However, a comparison of their R^2 values suggests that the superior model provides that fit compared to the other and whether the adsorption process within the system is more accurately characterized by either a monolayer or multilayer coverage of the adsorbate on the outer surface of the biochar.

(ii)   Kinetic Studies

The adsorption of iron metal ions onto biochar derived from baobab seeds was investigated using the linear Lagergren pseudo-first-order and pseudo-second-order kinetic models. The primary factor influencing adsorption is the adsorbent's ability to remove heavy metals from water through physicochemical processes. Kinetic studies, including an examination of mechanisms like mass transfer, are essential for understanding the process. To validate the adsorption mechanism, a comparison of the most plausible kinetic models is deemed necessary (Vunain *et al.*, 2017).

Pseudo-First-Order Kinetic Model

The determination of the adsorption rate constant was done using the pseudo-first-order equation (13) (Rahim & Garba, 2016).

$$\frac{dq_e}{dt} = k_1 \left(q_e - q_t \right) \tag{13}$$

where q_e (mg/g) represents the amount adsorbate (iron) adsorbed at equilibrium, while q_t (mg/g) denotes the amount adsorbate (iron) adsorbed at time t (min). The rate constant for the Pseudo-first order reaction is denoted as k_1 (per min). When the equation is integrated under the boundary conditions $t = 0$ and $t = t$, $q = q_t$, it establishes the relationship between for the Pseudo-first order kinetics and becomes equation (14) (Rahim & Garba, 2016).

$$Log\ (q_e - q_t) = Log\ q_e\ - \left(\frac{k_1}{2.303}\right)t \qquad\qquad (14)$$

In the study, the determination of the first-order rate constant (k_1) and equilibrium adsorption capacity (q_e) involved analyzing the slope and intercepts of a graph. Determining K_1 helps in understanding how quickly the adsorbate molecules are being captured by the adsorbent. Higher values of K_1 indicate faster adsorption kinetics (Rahim & Garba, 2016).

Pseudo-Second-Order Kinetic Model

The study employed also the pseudo-second-order kinetics equation which represents the reaction's rate law, to comprehensively describe the adsorption mechanism of metal ions (specifically iron) a solution (water) as in equation (15). The kinetic model aims to capture all stages during the adsorption process. The resulting equation (16), presented in its linear form, was utilized to define the rate law according to Rahim & Garba. (2016).

$$\frac{dq_t}{dt} = k_2\ (q_e\ - q_t)^2 \qquad\qquad (15)$$

$$\frac{t}{q_t} = \frac{1}{k_2 q_e{}^2}\ + \frac{1}{q_e}t \qquad\qquad (16)$$

The constants, k_2 (pseudo-second-order kinetic rate constant) and q_e (adsorption capacity at equilibrium), were determined. Determining K_2 helps in understanding the rate at which adsorbate molecules are released back into the solution from the adsorbent surface. Lower values of K_2 indicate slower desorption kinetics (Rahim & Garba, 2016).

3.4.6   Statistical Analysis

The data obtained from the experiment's procedures were analyzed utilizing the IBM SPSS version 27.0 software. Each experiment was conducted three times for accuracy. The mean and standard deviations were calculated to assess the effectiveness of baobab seeds-derived biochar for removal of iron from groundwater.

CHAPTER FOUR

RESULTS AND DISCUSSION

4.1   Results

In this study, groundwater collected during rainy and dry seasons from 19 boreholes located in Mpanda District were assessed. This addressed the first objective of the study, focusing on understanding the groundwater quality and its seasonal variations. Additionally, the study investigated the efficacy of baobab seeds-derived biochar in removing iron from groundwater, which fulfilled the second objective.

4.1.1   Physicochemical Parameters and Heavy Metal Concentrations

(i)   Descriptive Statistics

The descriptive statistics i.e., minimum, maximum, mean, and standard error for pH, temperature, dissolved oxygen, EC, TDS, turbidity, hardness, chloride, iron, manganese, lead, arsenic, and mercury are presented in details in Table 2. The water quality values were compared with those of WHO (WHO, 2011) and TBS (TBS, 2018) (see Table 2) to ensure compliance with health guidelines, identify potential risks, and highlight areas for improvement, thereby safeguarding public health.

pH Levels

pH levels were slightly higher (6.65 ± 0.07) in the rainy season compared with the dry season (6.22 ± 0.06) (Table 2). Majority of the boreholes had pH values below safe limit value (6.5) recommended by WHO and TBS (Fig. 3a).

Total Dissolved Solids (TDS) and Electrical Conductivity (EC)

Total Dissolved Solids levels ranged from 131.00 to 1237.00 mg/L, with the overall mean higher in the dry season (465.98 ± 35.28 mg/L) than in the rainy season (378.53 ± 31.61 mg/L). Similarly, electrical conductivity levels ranged from 260 to 2474.00 µS/cm, with a higher mean in the dry season (931.61 ± 70.59 µS/cm) compared to the rainy season (757.00 ± 63.23 µS/cm) (Table 2). Total Dissolved Solids and EC in B14 exceeded acceptable values given by WHO and TBS in both seasons (Fig. 3b and Fig. 3d). However, EC in B05 and B07 exceeded permissible values set by WHO and TBS in the dry season (Table 2 and Fig. 3d).

Dissolved Oxygen (DO)

Dissolved Oxygen levels ranged from 2.39 to 5.08 mg/L, with mean levels of 3.75 ± 0.07 mg/L in the rainy season and 3.30 ± 0.07 mg/L in the dry season (Table 2). Generally, the DO levels in groundwater appeared to be below 5 mg/L for both seasons (Fig. 3c).

Temperature

Temperature ranged from 22.33 to 31.60 °C, with a slightly higher mean value in the dry season $(28.02 \pm 0.19$ °C) compared with the rainy season $(26.76 \pm 0.22$ °C) (Table 2). The temperature in most boreholes exceeded the WHO limit of 25 °C (Fig. 3e) with the highest temperature recorded at B06 (31.6 °C) during dry season.

Turbidity Levels

Turbidity levels ranged from 2.00 to 14.60 NTU, with mean of 7.65 ± 0.54 NTU in the rainy season, and 8.03 ± 0.64 NTU in the dry season (Table 2). Turbidity levels in the twelve (12) boreholes exceeded the WHO and TBS maximum recommended value (5 NTU) (Fig. 3f).

Total Hardness

Total hardness concentrations ranged from 101.80 to 1425.00 mg/L, with higher mean values observed during the dry season $(317.94 \pm 37.50$ mg/L) compared with the rainy season $(284.21 \pm 36.02$ mg/L) (Table 2). The highest total hardness concentration was observed at BH14 for both seasons (Fig. 3g).

Chloride

Chloride concentrations were higher in the dry season $(57.14 \pm 9.61$ mg/L) compared with the rainy season $(49.60 \pm 8.44$ mg/L) (Table 2). B14 had the greatest concentration of chloride in both seasons (Fig. 3h).

Iron (Fe)

Iron concentrations in most boreholes exceeded WHO and TBS allowable limits of 0.3 mg/L (Fig. 4a). The Fe concentrations ranged from 0.08 to 5.78 mg/L, with the mean value of 1.84 ± 0.21 mg/L in the rainy season and 2.19 ± 0.23 mg/L in the dry season (Table 2).

Manganese (Mn)

Manganese concentrations exceeded WHO and TBS allowable limits of 0.1 mg/L in most of the boreholes (Fig. 4b). The manganese concentrations ranged from 0.02 to 0.53 mg/L, with mean values of 0.24 ± 0.01 mg/L and 0.27 ± 0.01 mg/L in the rainy and dry seasons, respectively (Table 2).

Lead (Pb)

Lead concentrations ranged from 3.34 to 99.34 µg/L, with a mean value of 25.58 ± 4.16 µg/L in the rainy season and 30.06 ± 4.65 µg/L in the dry season (Table 2). The concentrations of Pb from 6 boreholes exceeded WHO and TBS maximum allowable limit of 10 µg/L (Fig. 4c).

Mercury (Hg)

The concentrations of Hg ranged from 0.20 to 3.71 µg/L with mean values of 1.75 ± 0.12 µg/L in the rainy and 1.95 ± 0.12 µg/L in the dry season (Table 2). All boreholes had concentrations of Hg and as within the maximum allowable values set by WHO and TBS standards of 6 µg/L and 10 µg/L, respectively (Fig. 4d).

Arsenic (As)

The concentrations of as ranged from 0.16 to 8.06 µg/L, with mean values of 3.35 ± 0.22 µg/L in the rainy and 3.34 ± 0.25 µg/L in the dry season (Table 2). All boreholes had concentrations of as within the maximum allowable values set by WHO and TBS standards of 6 µg/L and 10 µg/L, respectively (Fig. 4e).

Table 2: **Physicochemical parameters and heavy metal concentrations in groundwater from 19 boreholes in Mpanda district for the rainy and dry seasons and the WHO and TBS maximum allowable limits. Min = Minimum, Max = Maximum, SE = Standard error of the mean**

Parameters	Rainy season (n=57)				Dry season (n=57)				WHO (WHO, 2011)	TBS (TBS, 2018)
	Min	Max	Mean	SE	Min	Max	Mean	SE		
pH	5.61	7.60	6.65	0.07	5.48	7.22	6.22	0.06	6.5-8.5	6.5-8.5
DO (mg/L)	3.03	5.08	3.75	0.07	2.39	4.34	3.30	0.07	-	-
TDS (ppm)	131.00	1191.00	378.53	31.61	159.00	1237.00	465.98	35.28	1000	1000
EC (µS/cm)	260.00	2382.00	757.00	63.23	318.00	2474.00	931.61	70.59	1000	1500
Temp (°C)	22.20	30.50	26.76	0.22	25.50	31.60	28.02	0.19	25	-
Turbidity (NTU)	2.00	14.44	7.65	0.54	3.02	14.60	8.03	0.64	5	5
Hardness (mg/L)	101.80	1342.00	284.21	36.02	103.86	1425.00	317.94	37.50	300	300
Cl (mg/L)	15.22	280.10	49.60	8.44	17.44	329.50	57.14	9.61	250	250
Fe (mg/L)	0.08	5.36	1.84	0.21	0.14	5.78	2.19	0.23	0.3	0.3
Mn (mg/L)	0.02	0.53	0.24	0.01	0.03	0.53	0.27	0.01	0.1	0.1
Pb (µg/L)	3.34	95.31	25.58	4.16	4.15	99.34	30.06	4.65	10	10
Hg (µg/L)	0.20	3.40	1.75	0.12	0.50	3.71	1.95	0.12	6	10
As (µg/L)	0.50	7.50	3.35	0.22	0.16	8.06	3.34	0.25	10	10
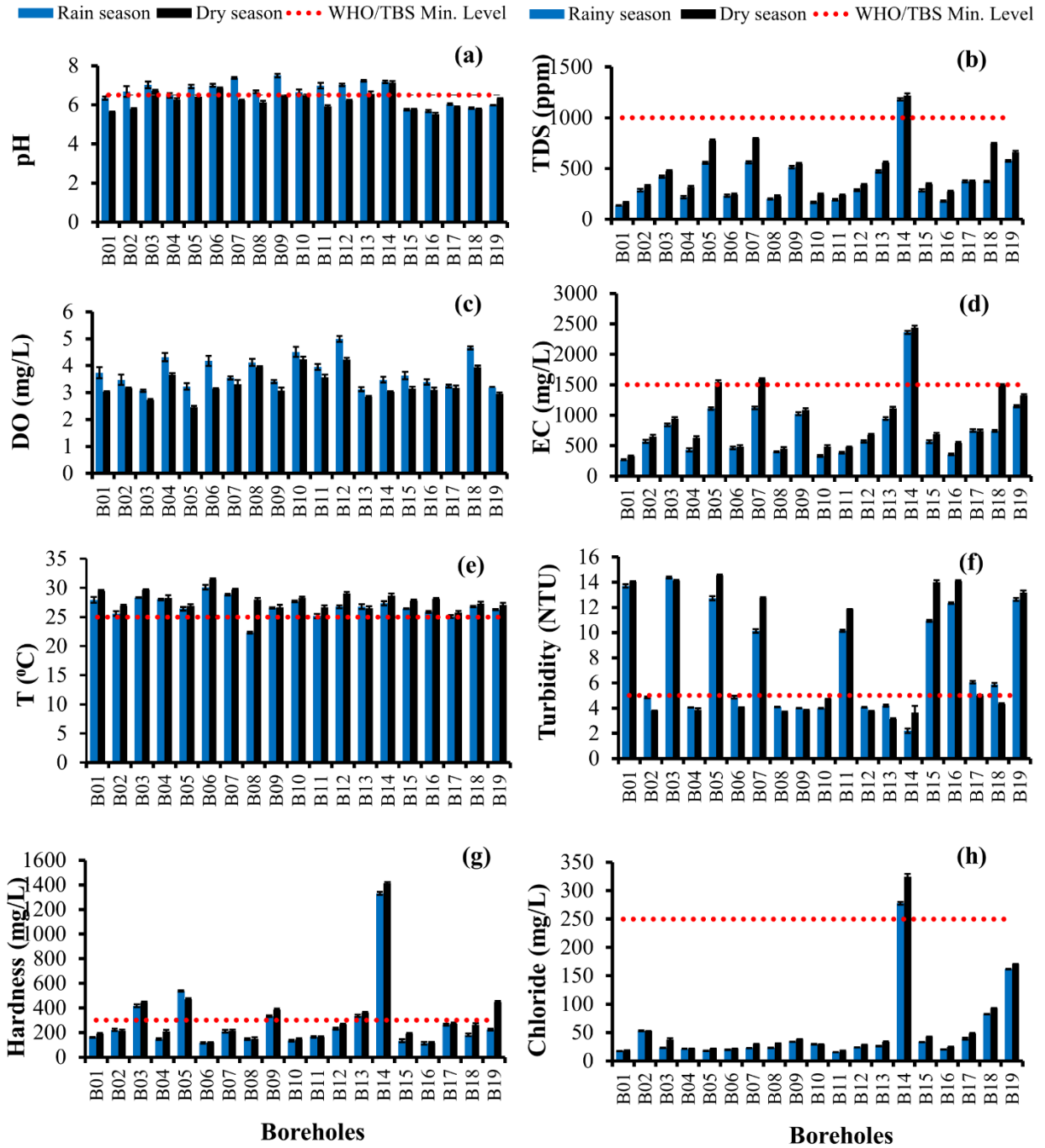
Figure 3: **Variations in mean values of pH, TDS, DO, EC, temperature, turbidity, hardness and chloride in the 19 boreholes in Mpanda district for the rainy and dry seasons. The bars denote the standard error of the mean**
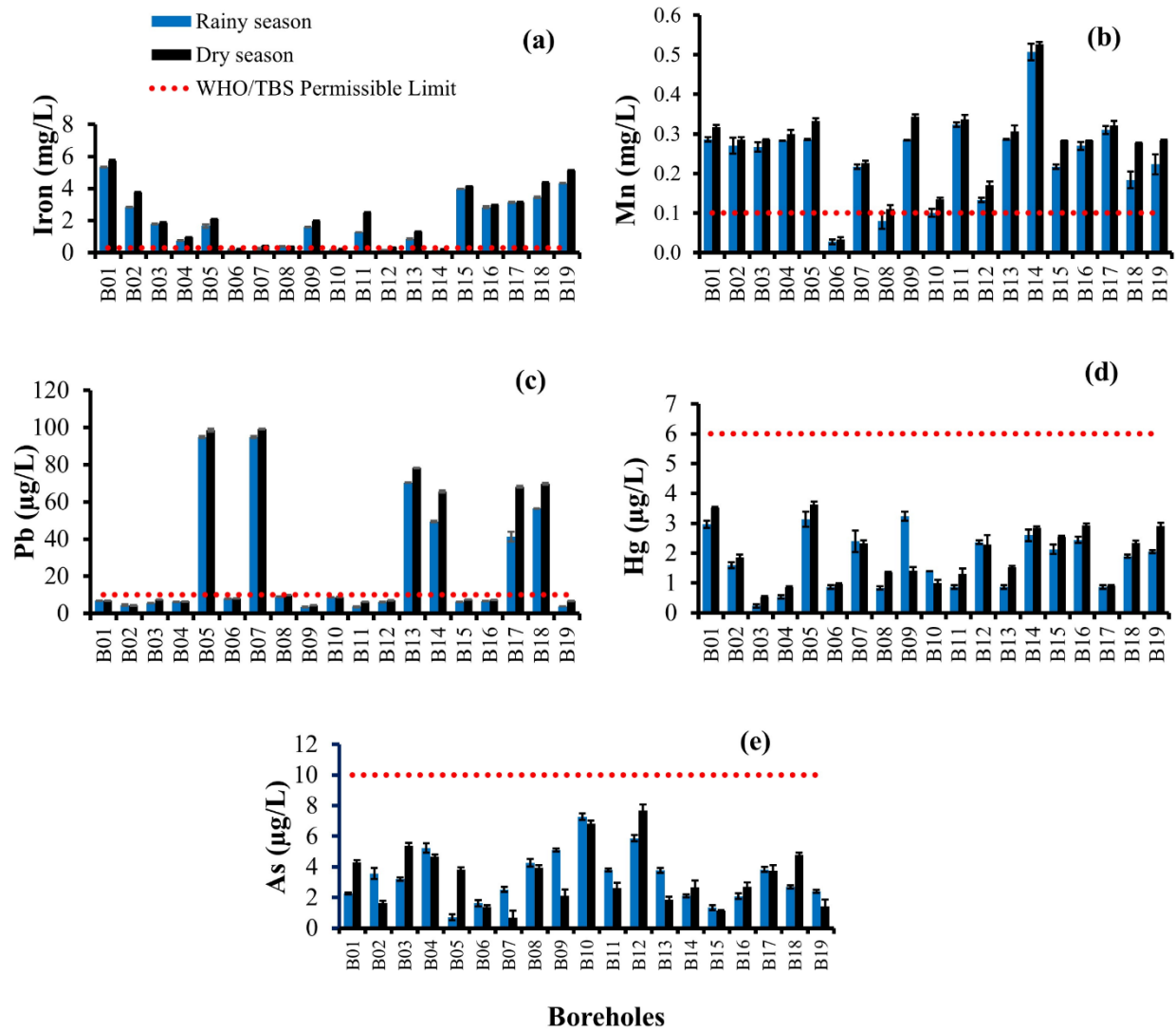
Figure 4: **Variations in mean values for the Fe, Mn, Pb, Hg and As in the 19 boreholes in Mpanda district for the rainy and dry seasons. The bars denote the standard error of the mean**

(ii) **Comparative Analysis of Water Quality Parameters Across Seasons and Groups**

There was a significant seasonal variation in all water quality parameters across the study area, with distinct patterns observed between rainy and dry seasons t-tests $p < 0.05$, except for turbidity and arsenic (Wilcoxon signed rank test, Table 5). In addition, there was significant differences in all water quality parameters across 19 boreholes ($p < 0.01$, Table 3). Table 4 shows the significant difference across the 4 groups. The statistically significant difference was observed for pH, DO, TDS, EC, turbidity, hardness, chloride, Fe and As ($p < 0.05$) for rainy season while pH, DO, turbidity, hardness, chloride, Fe and Hg ($p < 0.05$) for dry season.

36

Table 3: **The Kruskal-Wallis Test results indicating differences across 19 boreholes for physicochemical parameters and heavy metal concentrations in Mpanda district. K = Kruskal-Wallis statistics, N = number of water sampling, Df = degree of freedom**

Variable	Rainy season (N=57)			Dry season (N=57)		
	Df	K statistics	p-value	K statistics	Df	p-value
pH	18	53.556	0.000	55.033	18	0.000
DO (mg/L)	18	53.546	0.000	53.029	18	0.000
TDS (ppm)	18	55.412	0.000	55.376	18	0.000
EC (μS/cm)	18	54.178	0.000	55.376	18	0.000
Temp (°C)	18	54.178	0.000	53.561	18	0.000
Turb (NTU)	18	55.599	0.000	54.433	18	0.000
Hard (mg/L)	18	55.151	0.000	55.366	18	0.000
Cl (mg/L)	18	55.785	0.000	55.680	18	0.000
Fe (mg/L)	18	55.607	0.000	55.746	18	0.000
Mn (mg/L)	18	53.896	0.000	55.131	18	0.000
Pb (μg/L)	18	55.504	0.000	55.760	18	0.000
Hg (μg/L)	18	54.608	0.000	55.086	18	0.000
As (μg/L)	18	55.148	0.000	54.774	18	0.000

The variation is statistically significant at $p < 0.05$

Table 4: **The Kruskal-Wallis Test results indicating differences across 4 groups of boreholes in physicochemical parameters and heavy metal concentrations. K= Kruskal-Wallis Statistic, N = number of sampling, Df = degree of freedom**

Parameter	Df	Rainy season (N = 57)		Dry season (N =57)	
		K	*p*-value	K	*p*-value
pH	3	32.197	0.000	37.375	0.000
DO (mg/L)	3	9.736	0.021	10.282	0.016
TDS (ppm)	3	8.249	0.041	3.942	**0.268**
EC (µS/cm)	3	8.249	0.041	3.903	**0.272**
Temp (°C)	3	9.701	**0.21**	2.230	**0.526**
Turb (NTU)	3	13.510	0.004	10.946	0.012
Hard (mg/L)	3	17.466	0.001	9.398	0.024
Cl (mg/L)	3	11.261	0.01	18.449	0.000
Fe (mg/L)	3	33.735	0.000	36.790	0.000
Mn (mg/L)	3	5.207	**0.157**	4.773	**0.189**
Pb (µg/L)	3	3.862	**0.277**	4.782	**0.188**
Hg (µg/L)	3	5.209	**0.157**	17.099	0.001
As (µg/L)	3	11.117	0.011	3.700	**0.296**

The variation is statistically significant at $p < 0.05$, The bold value indicates no significant variation ($p > 0.05$)

Table 5:   **The Related-Samples Wilcoxon signed-rank test results indicating differences between rainy and dry seasons for physicochemical parameters and heavy metal concentrations for 19 borehole sites in Mpanda district. W = Wilcoxon signed-rank statistics, p = p-values**

Parameters	Wilcoxon signed-rank test (N = 57)	
	W statistics	**p-value**
pH	74.000	0.000
DO (mg/L)	0.000	0.000
TDS (ppm)	1641.000	0.000
EC (µS/cm)	1641.000	0.000
Temp (°C)	1611.500	0.000
Turb (NTU)	1018.500	0.127
Hard (mg/L)	1411.000	0.000
Cl (mg/L)	1576.000	0.000
Fe (mg/L)	1588.000	0.000
Mn (mg/L)	1428.000	0.000
Pb (µg/L)	1630.000	0.000
Hg (µg/L)	1331.000	0.000
As (µg/L)	781.000	0.718

The variation is statistically significant at $p < 0.05$

Tables 6, 7, and 8 present the post hoc test results, indicating differences across specific groups for various water quality parameters in the rainy and dry seasons. In the rainy season, the pH parameter showed significant differences specifically between Ilembo and Kakese ($K = -18.32$, $p < 0.01$), Magamba and Kakese ($K = -23.74$, $p < 0.01$), Ilembo and Sitalike ($K = -31.38$, $p < 0.01$), and Magamba and Sitalike ($K = -13.06$, $p < 0.05$). Similarly, in the dry season, pH levels also showed significant differences between Ilembo and Kakese ($K = -29.03$, $p < 0.01$), Ilembo and Sitalike ($K = -30.93$, $p < 0.01$), Magamba and Kakese ($K = -18.21$, $p < 0.01$), and Magamba and Sitalike ($K = -20.11$, $p < 0.01$).

For Dissolved Oxygen (DO) in the rainy season, significant differences were noted between Sitalike and Magamba ($K = 14.70$, $p < 0.05$) and Sitalike and Kakese ($K = -18.66$, $p < 0.05$), while in the dry season, differences were significant between Sitalike and Magamba ($K = -20.01$, $p < 0.05$) and Ilembo and Magamba ($K = -12.88$, $p < 0.05$). Total Dissolved Solids (TDS) and Electrical Conductivity (EC) differed significantly in the rainy season between Kakese and Sitalike ($K = 15.98$, $p < 0.05$) and Sitalike and Kakese ($K = -14.18$, $p < 0.05$), with no significant differences observed in the dry season.

Temperature showed significant differences in the rainy season between Ilembo and Kakese ($K = -17.99$, $p < 0.01$) and Magamba and Kakese ($K = -17.83$, $p < 0.05$), but no significant differences in the dry season. Turbidity differed significantly in the rainy season between Sitalike and Ilembo ($K = 19.80$, $p < 0.01$) and Kakese and Ilembo ($K = 16.58$, $p < 0.01$), and in the dry season between Sitalike and Ilembo ($K = 19.02$, $p < 0.01$).

Hardness exhibited significant differences in the rainy season between Kakese and Sitalike ($K = 21.90$, $p < 0.01$) and Ilembo and Sitalike ($K = -21.23$, $p < 0.01$), and in the dry season between Kakese and Sitalike ($K = 17.27$, $p < 0.01$) and Ilembo and Sitalike ($K = -14.92$, $p < 0.05$). Chloride differences were significant in the rainy season between Kakese and Ilembo ($K = 17.17$, $p < 0.05$) and Kakese and Sitalike ($K = 17.97$, $p < 0.05$), and in the dry season between Kakese and Ilembo ($K = 21.44$, $p < 0.01$), Kakese and Sitalike ($K = 24.00$, $p < 0.01$), and Magamba and Sitalike ($K = -14.92$, $p < 0.05$).

Iron (Fe) exhibited significant differences in the rainy season between Kakese and Ilembo ($K = 30.92$, $p < 0.01$), Sitalike and Ilembo ($K = 26.13$, $p < 0.01$), and Kakese and Sitalike ($K = 4.78$, $p < 0.01$), and in the dry season between Kakese and Ilembo ($K = 32.00$, $p < 0.01$), Sitalike and Ilembo ($K = 29.00$, $p < 0.01$), and Magamba and Ilembo ($K = 22.00$, $p < 0.01$). For Mercury (Hg), there was no significant difference in the rainy season, but significant differences in the dry season were observed between Kakese and Ilembo ($K = 20.93$, $p < 0.01$), Sitalike and Ilembo ($K = 29.00$, $p < 0.01$), and Magamba and Ilembo ($K = 17.97$, $p < 0.01$).

Lastly, Arsenic (As) showed significant differences in the rainy season between Ilembo and Sitalike ($K = -18.32$, $p < 0.01$) and Ilembo and Magamba ($K = -23.74$, $p < 0.01$), with no significant differences in the dry season. These results also indicate notable seasonal variations in water quality parameters across different borehole groups.

Table 6: **Post hoc test pairwise comparisons results indicating differences across specific groups in physicochemical parameters (Ph, dissolved oxygen (DO), total dissolved solids (TDS and electrical conductivity (EC)). K= Kruskal-Wallis Statistic, N = number of sampling, DO = dissolved solids, TDS = total dissolved solids. Group1 = Ilembo ward, group2 = Magamba ward, group3 = Sitalike ward and group4 = Kakese ward**

Sample 1-Sample 2	Rainy season (N = 57)		Sample 1-Sample 2	Dry season (N =57)	
	K statistic	*p*-value		K	*p*-value
pH					
Group1-Group4	-18.319	0.003	Group1-Group2	-10.819	**0.080**
Group1-Group2	-23.736	0.000	Group1-Group4	-29.028	0.000
Group1-Group3	-31.378	0.000	Group1-Group3	-30.928	0.000
Group4-Group2	5.417	**0.424**	Group2-Group4	-18.208	0.007
Group4-Group3	13.058	0.042	Group2-Group3	-20.108	0.002
Group2-Group3	-7.642	**0.234**	Group4-Group3	1.900	**0.768**
Dissolved oxygen					
Group3-Group1	9.006	**0.121**	Group3-Group1	7.133	**0.219**
Group3-Group2	14.700	0.022	Group3-Group4	-11.883	**0.064**
Group3-Group4	-18.658	0.004	Group3-Group2	20.008	0.002
Group1-Group2	-5.694	**0.357**	Group1-Group4	-4.750	**0.442**
Group1-Group4	-9.653	**0.119**	Group1-Group2	-12.875	0.037
Group2-Group4	-3.958	**0.559**	Group4-Group2	8.125	**0.230**
Total dissolved solids					
Group4-Group1	1.806	**0.770**	***	***	***
Group4-Group2	7.792	**0.250**	***	***	***
Group4-Group3	15.983	0.013	***	***	***
Group1-Group2	-5.986	**0.333**	***	***	***
Group1-Group3	-14.178	0.015	***	***	***
Group2-Group3	-8.192	**0.770**	***	***	***
Electrical conductivity					
Group4-Group1	1.806	**0.770**	***	***	***
Group4-Group2	7.792	**0.250**	***	***	***
Group4-Group3	15.983	0.013	***	***	***
Group1-Group2	-5.986	**0.333**	***	***	***
Group1-Group3	-14.178	0.015	***	***	***
Group2-Group3	-8.192	**0.203**	***	***	***

The variation is statistically significant at p < 0.05, *** indicates no multiple comparisons were performed as the overall test did not show significant differences across samples. The bold value indicates no significant variation (p > 0.05)

Table 7: **Post hoc test pairwise comparisons results indicating differences across specific groups in physicochemical parameters (temperature, turbidity, hardness and chloride). K= Kruskal-Wallis Statistic, N= number of sampling. Group1 = Ilembo ward, group2 = Magamba ward, group3 = Sitalike ward and group4 = Kakese ward**

Sample 1-Sample 2	Rainy season (N = 57)		Sample 1-Sample 2	Dry season (N =57)	
	K statistic	*p*-value		K	*p*-value
	Temperature				
Group1-Group2	-.903	**0.884**	***	***	***
Group1-Group3	-5.578	**0.336**	***	***	***
Group1-Group4	-17.986	0.004	***	***	***
Group2-Group3	-4.675	**0.467**	***	***	***
Group2-Group4	-17.083	0.012	***	***	***
Group3-Group4	-12.408	**0.053**	***	***	***
	Turbidity				
Group3-Group4	-3.217	**0.617**	Group3-Group2	10.558	**0.10**
Group3-Group2	9.675	**0.132**	Group3-Group4	-12.850	**0.05**
Group3-Group1	19.800	0.001	Group3-Group1	19.017	0.00
Group4-Group2	6.458	**0.340**	Group2-Group4	-2.292	**0.735**
Group4-Group1	16.583	0.007	Group2-Group1	8.458	**0.171**
Group2-Group1	10.125	**0.102**	Group4-Group1	6.167	**0.319**
	Hardness				
Group4-Group1	0.667	**0.914**	Group4-Group1	2.278	**0.713**
Group4-Group2	12.000	**0.077**	Group4-Group2	5.083	**0.453**
Group4-Group3	21.900	0.001	Group4-Group3	17.267	0.007
Group1-Group2	-11.333	**0.067**	Group1-Group2	-2.806	**0.650**
Group1-Group3	-21.233	0.000	Group1-Group3	-14.989	0.010
Group2-Group3	-9.900	**0.124**	Group2-Group3	-12.183	**0.058**
	Chloride				
Group4-Group2	6.417	**0.34**	Group4-Group2	9.083	**0.18**
Group4-Group1	17.167	0.01	Group4-Group1	21.444	0.00
Group4-Group3	17.967	0.01	Group4-Group3	24.000	0.00
Group2-Group1	10.750	**0.08**	Group2-Group1	12.361	**0.05**
Group2-Group3	-11.550	**0.07**	Group2-Group3	-14.917	0.02
Group1-Group3	-.800	**0.89**	Group1-Group3	-2.556	**0.66**

The variation is statistically significant at p < 0.05, *** indicates no multiple comparisons were performed as the overall test did not show significant differences across samples. The bold value indicates no significant variation (p > 0.05)

Table 8: **Post hoc test pairwise comparisons results indicating differences across specific groups in heavy metals (iron (Fe), mercury (Hg) and arsenic (As)). K= Kruskal-Wallis Statistic, n = number of sampling sites, DO = dissolved solids, TDS = total dissolved solids. Group1 = Ilembo ward, group2 = Magamba ward, group3 = Sitalike ward and group4 = Kakese ward**

Sample 1-Sample 2	Rainy season (*N* = 19)		Sample 1-Sample 2	Dry season (*N* =19)	
	K statistic	*p*-value		K	*p*-value
	Iron				
Group4-Group3	4.783	**0.46**	Group4-Group3	3.000	**0.64**
Group4-Group2	6.625	**0.33**	Group4-Group2	10.000	**0.14**
Group4-Group1	30.917	0.00	Group4-Group1	32.000	0.00
Group3-Group2	1.842	**0.77**	Group3-Group2	7.000	**0.28**
Group3-Group1	26.133	0.00	Group3-Group1	29.000	0.00
Group4-Group3	4.783	0.00	Group2-Group1	22.000	0.00
	Mercury				
Group4-Group3	***	***	Group4-Group3	1.492	**0.82**
Group4-Group2	***	***	Group4-Group2	2.958	**0.66**
Group4-Group1	***	***	Group4-Group1	20.931	0.00
Group3-Group2	***	***	Group3-Group2	1.467	**0.82**
Group3-Group1	***	***	Group3-Group1	19.439	0.00
Group2-Group1	***	***	Group2-Group1	17.972	0.00
	Arsenic				
Group1-Group4	-9.528	**0.123**	***	***	***
Group1-Group3	-14.961	0.010	***	***	***
Group1-Group2	-18.611	0.003	***	***	***
Group4-Group3	5.433	**0.398**	***	***	***
Group4-Group2	9.083	**0.180**	***	***	***
Group3-Group2	3.650	**0.570**	***	***	***

The variation is statistically significant at p < 0.05, *** indicates no multiple comparisons were performed as the overall test did not show significant differences across samples.

(iii) Correlational Analysis

The Spearman's rank-order correlation matrix between physicochemical parameters and heavy metals is presented in Table 9. There was a significant and strong negative correlation ($r = -0.73$, $p \leq 0.01$) and ($r = -0.69$, $p \leq 0.01$) between pH and Fe for the rainy and dry seasons respectively. DO was moderately and negatively ($r = -0.50$, $p \leq 0.01$) and ($r = -0.52$, $p \leq 0.01$) correlated with Mn. Turbidity and Fe were strongly and positively ($r = 0.68$, $p \leq 0.01$) and ($r = 0.71$, $p \leq 0.01$) correlated. Total hardness and Mn were moderately and positively ($r = 0.59$, $p \leq 0.01$) and ($r = 0.56$, $p \leq 0.01$) correlated.

Table 9: Spearman's rank-order correlation of physicochemical parameters and heavy metal concentrations in groundwater for the 19 boreholes in Mpanda district for both the rainy and dry seasons

	pH	DO	TDS	EC	Temp	Turb	Hard	Cl	Fe	Mn	Pb	Hg	As
Rainy season													
pH	1.00												
DO	-0.13	1.00											
TDS	0.42*	-0.53**	1.00										
EC	0.43**	-0.53**	1.00**	1.00									
Temp	0.35**	0.17	0.09	0.09	1.00								
Turb	-0.37**	-0.45**	-0.02	-0.02	-0.06	1.00							
Hard	0.52**	-0.57**	0.77**	0.77**	-0.03	-0.03	1.00						
Cl	-0.10	-0.12	0.49**	0.50**	-0.19	-0.39**	0.34*	1.00					
Fe	-0.73**	-0.37**	-0.05	-0.05	-0.35**	0.68**	-0.03	0.11	1.00				
Mn	0.15	-0.50**	0.25	0.25	-0.22	0.08	0.54**	-0.02	0.19	1.00			
Pb	0.11	-0.00	0.22	0.22	0.21	-0.05	0.13	-0.03	-0.26*	-0.03	1.00		
Hg	0.07	-0.08	0.25	0.25	-0.01	0.06	0.21	0.07	0.15	0.15	0.10	1.00	
As	0.20	0.33*	-0.24	-0.24	-0.11	-0.57**	0.02	0.14	-0.32*	-0.09	-0.28*	-0.36**	1.00
Dry season													
pH	1.00												
DO	-0.31*	1.00											
TDS	0.35**	-0.41**	1.00										
EC	0.35**	-0.40*	1.00**	1.00									
Temp	0.19	0.09	-0.19	-0.19	1.00								
Turb	-0.25	-0.39**	0.05	0.05**	0.13	1.00							
Hard	0.44**	-0.54**	0.80**	0.80**	-0.28*	-0.01	1.00						
Cl	0.12	-0.15**	0.58**	0.57	-0.27*	-0.21	0.51**	1.00					
Fe	-0.69**	-0.26	0.00*	0.00	-0.43**	0.71**	0.07	0.16	1.00				
Mn	0.08	-0.52**	0.32	0.33**	-0.45**	0.14	0.56**	0.04	0.25	1.00			
Pb	0.23	-0.11	0.46**	0.46**	0.07	0.08	0.18	0.13	-0.27*	-0.14	1.00		
Hg	-0.32*	-0.31*	0.29*	0.29*	0.01	0.32*	0.18	0.06	0.39**	0.16	0.12	1.00	
As	0.00	0.33*	-0.24	-0.23	0.14	-0.05	0.04	-0.23	-0.16	-0.04	0.00	-0.24	1.00

* Correlation is significant at $p \leq 0.05$ level, ** Correlation is significant at $p \leq 0.01$ level

(iv)   Principal Component Analysis (PCA)

The PCA for both the physicochemical parameters and heavy metal concentrations is presented in Fig. 5. The first four principal components had eigen values ranging from 4.87 to 1.04. The first two components collectively explained the total variation in the physicochemical and heavy metal concentrations (Table 10 and Fig. 5). Factor loadings ≥ 0.75 were considered high, 0.50 to 0.75 were considered moderate, and 0.30 to 0.50 were considered weak (Rahman *et al*., 2018). The presence of four principal components was confirmed by the Scree plot (Fig. 5), where eigenvalues were greater than 1.

Component 1 (36.56% variation explained) showed high loadings in TDS, EC, hardness, chloride, and manganese. Component 2 (21.56% variation explained) demonstrated significant contributions from turbidity, decreased dissolved oxygen (DO), and arsenic. Component 3 (11.10% variation explained) featured loadings from pH and reduced iron. Component 4 (8.03% variation explained) was influenced by temperature and mercury.

Table 10:   **The load matrix results generated through the varimax method**

Parameters	Component			
	1	**2**	**3**	**4**
pH	0.13	0.86[*]	0.08	0.23
Dissolved oxygen (mg/L)	-0.21	0.26	-0.90[*]	0.06
Total dissolved solids (ppm)	0.93[*]	0.10	0.11	0.25
Electrical conductivity (μS/cm)	0.93[*]	0.10	0.11	0.25
T (°C)	-0.04	0.17	-0.08	0.74
Turbidity (NTU)	-0.29	-0.50[**]	0.64[**]	0.26
Hardness (mg/L)	0.89[*]	0.25	0.19	0.06
Chloride (mg/L)	0.92[*]	-0.15	-0.09	-0.06
Iron (mg/L)	-0.07	-0.86[*]	0.31	-0.08
Manganese (mg/L)	0.65[**]	-0.06	0.53[**]	-0.18
Lead (μg/L)	0.34	0.26	0.31	0.53[**]
Mercury (μg/L)	0.36	-0.37	0.02	0.45
Arsenic (μg/L)	-0.21	0.44	-0.54[**]	-0.45
Eigenvalues	4.75	2.79	1.45	1.09
Variance (%)	36.52	21.48	11.17	8.36
Cumulative (%)	36.52	58.01	69.18	77.54

Method of extraction: Principal component analysis
Rotation method: Varimax with Kaiser Normalisation
* High loading of > 0.75, ****** moderate loading
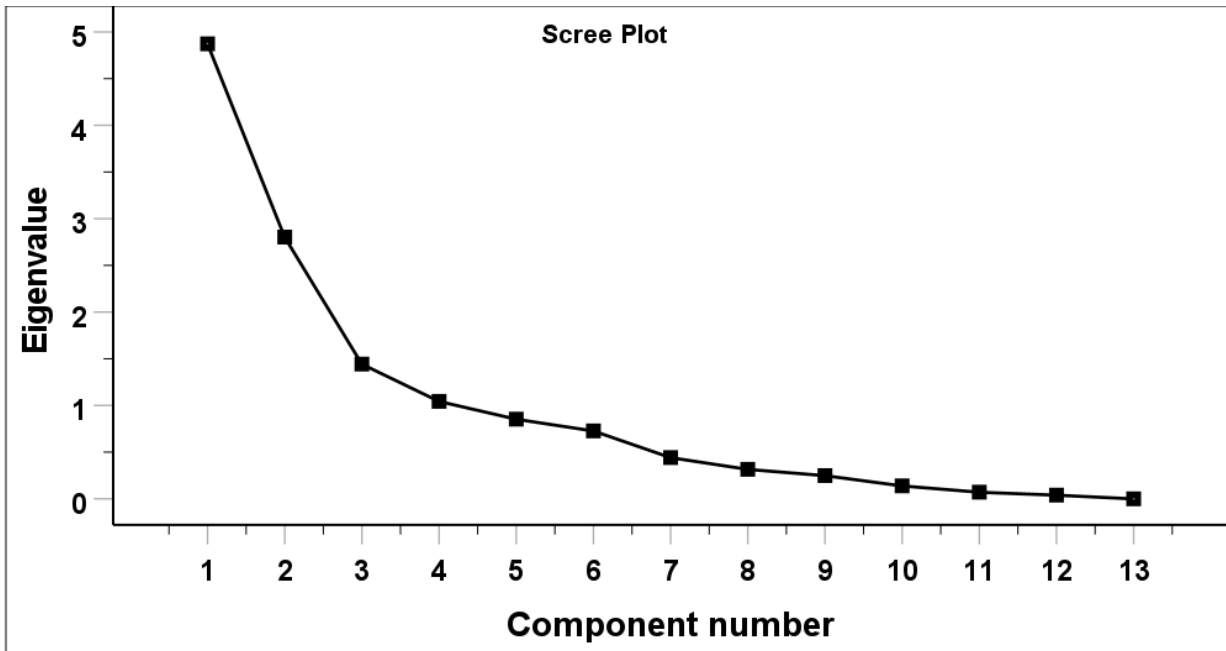
Figure 5: **Scree plot of physicochemical parameters and heavy metal concentrations**

(v) Water Quality Index (WQI)

The WQI ranged 50.72 to 242.28 (Fig. 6) visually presents the groundwater results for WQI in the rainy and dry seasons. Additionally, Tables 11, and 12 outline the relevant weight of parameters, water classification based on WQI, and WQI classification for individual water samples, respectively.

Table 11:   **The relevant weight of parameters**

Parameter	TBS Limits	Weight (wi)	Relative Weight (Wi)
pH	6.5	1	0.08
Dissolved oxygen (mg/L)	5	1	0.08
Total dissolved solids (ppm)	1000	1	0.08
Electrical conductivity (μS/cm)	1500	1	0.08
Temperature (°C)	25	1	0.08
Turbidity (NTU)	5	1	0.08
Hardness (mg/L)	300	1	0.08
Chloride (mg/L)	250	1	0.08
Iron (mg/L)	0.3	1	0.08
Manganese (mg/L)	0.1	1	0.08
Lead (μg/L)	10	1	0.08
Mercury (μg/L)	6	1	0.08
Arsenic (μg/L)	10	1	0.08
		$\sum = 13$	$\sum = 1.0$

Table 12: **Water quality indices for the groundwater from 19 boreholes in Mpanda District**

Borehole ID	WQI		Water Classification (Rahman *et al.*, 2018)	
	Rainy	Dry	Rainy	Dry
B01	216.92	232.54	Water unsuitable for drinking	Water unsuitable for drinking
B02	140.26	161.88	Poor water	Poor water
B03	119.65	141.97	Poor water	Poor water
B04	85.07	94.16	Good water	Good water
B05	204.73	228.67	Water unsuitable for drinking	Water unsuitable for drinking
B06	50.72	50.91	Good water	Good water
B07	152.57	167.08	Poor water	Poor water
B08	59.50	64.09	Good water	Good water
B09	117.81	128.59	Poor water	Poor water
B10	59.58	65.15	Good water	Good water
B11	107.20	143.87	Poor water	Poor water
B12	65.90	75.34	Good water	Good water
B13	145.18	163.29	Poor water	Poor water
B14	171.02	194.08	Poor water	Poor water
B15	171.39	189.42	Poor water	Poor water
B16	146.11	157.07	Poor water	Poor water
B17	181.59	202.27	Poor water	Water unsuitable for drinking
B18	198.25	242.28	Poor water	Water unsuitable for drinking
B19	193.58	229.83	Poor water	Water unsuitable for drinking

WQI < 50 = Excellent, 50 ≤ WQI ≤ 100 = Good, 100 < WQI ≤ 200 = Poor, 200 < WQI ≤ 300 = very poor, 300 < WQI ≤ 400 = Polluted and WQI >400 = Very polluted (Mihale, 2022)
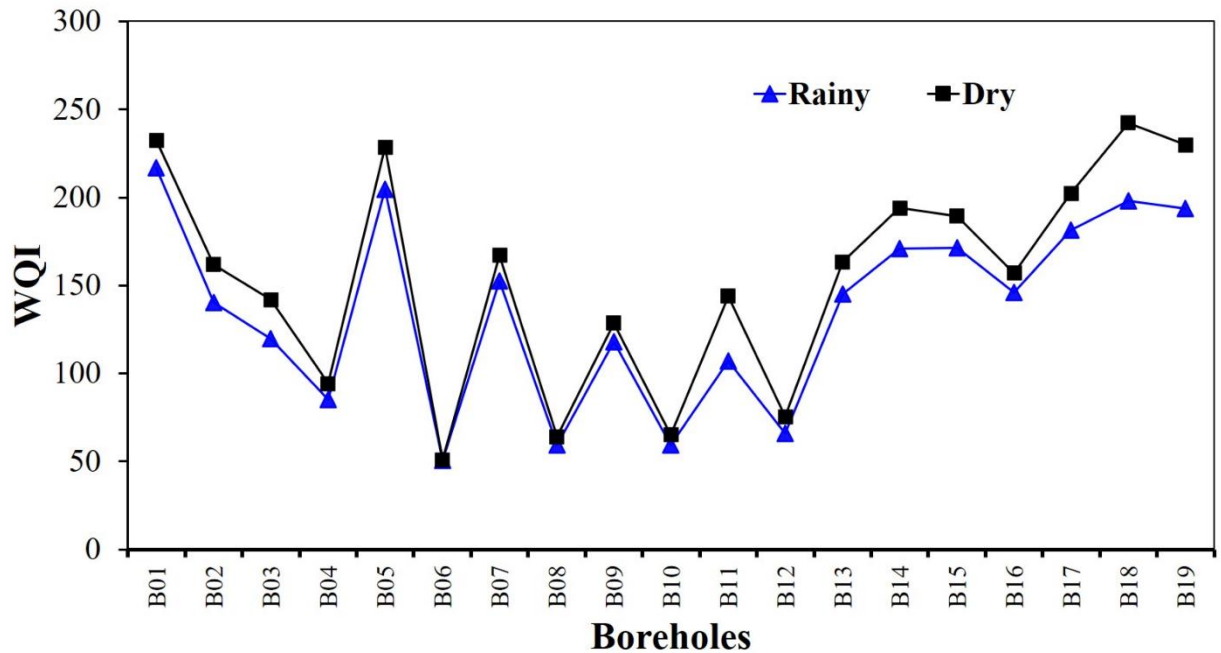
Figure 6: **Water quality indices (WQI) for 19 boreholes for the rainy and dry seasons**

4.1.2 Potential Use of Baobab Seeds to Remove Iron from Groundwater

(i) Characterization of Biochar Adsorbent

SEM-EDX Characterization

Scanning electron microscopy (SEM) analysis of biochar derived from baobab seeds, prepared at 700°C, revealed distinctive structural features, as depicted in Fig. 7. The SEM micrographs exhibited deep irregular voids, a rough surface, and varied morphology.

Furthermore, the Energy Dispersive X-ray (EDX) micrograph presented in Fig. 7 supplements the microscopic analysis by confirming the elemental composition of the biochar prepared from baobab seeds. Carbon constitutes the predominant element, comprising approximately 84.74%, followed by oxygen of 15.26% (Fig. 8).

50

Figure 7: **A and B Scanning electron microscopy (SEM) micrographs of baobab seed-derived biochar at 700 ºC**
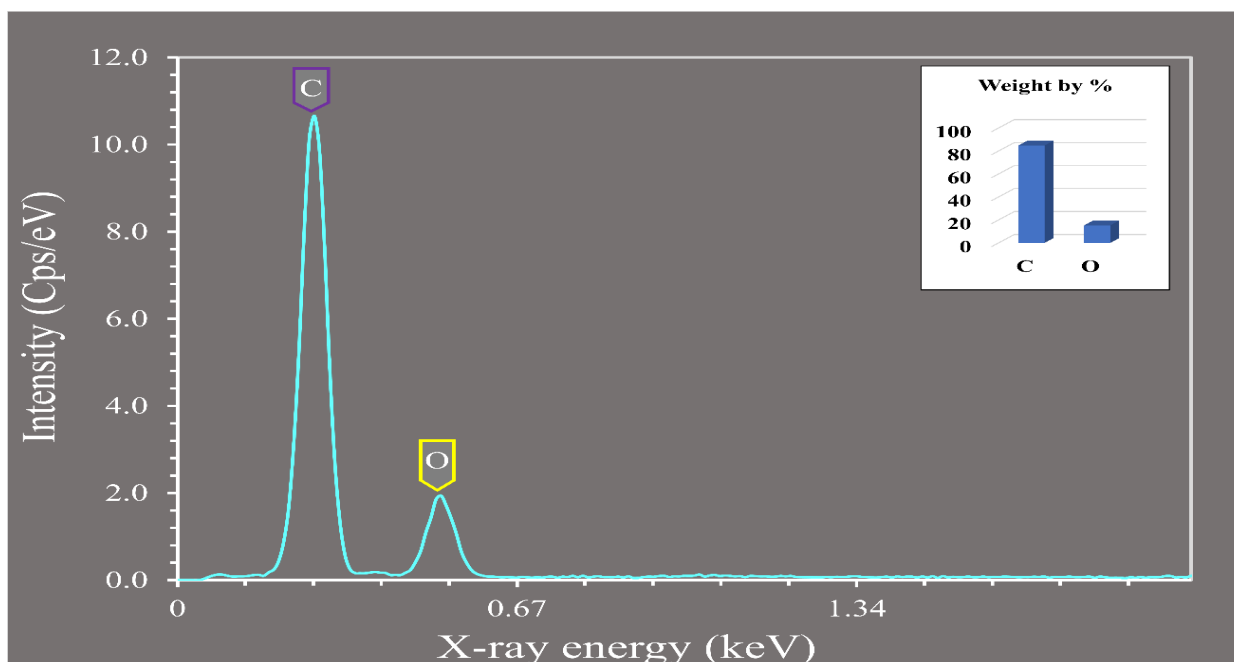
Figure 8: **EDX micrograph illustrating the existence of carbon and oxygen in the biochar derived from baobab seeds after pyrolysis at 700 ºC**
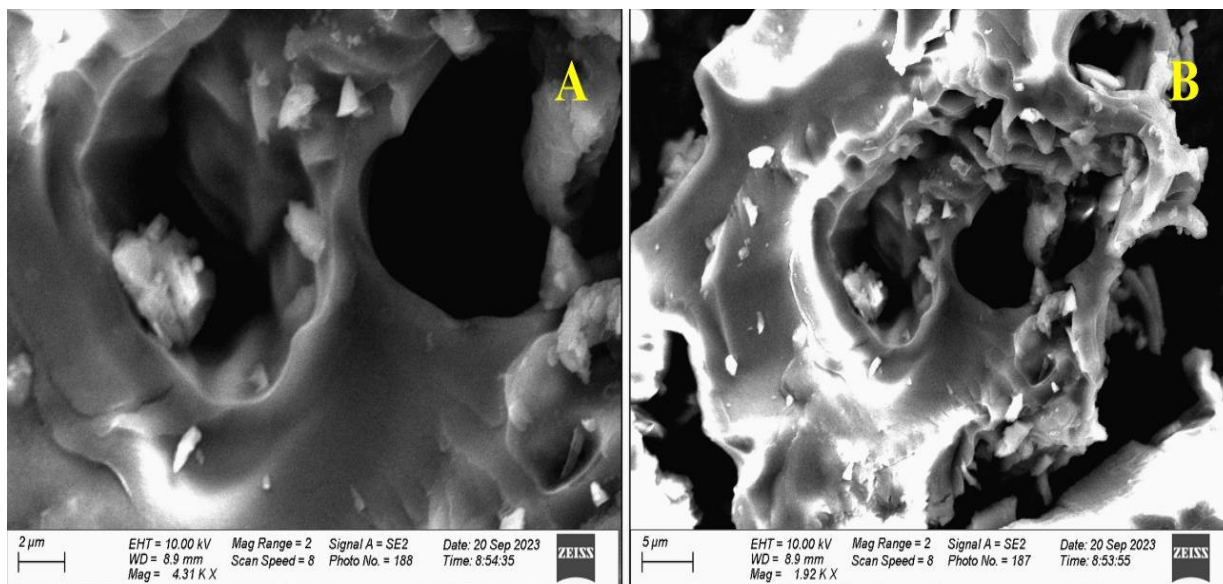
X-ray Diffraction (XRD) Characterization

The X-ray diffraction (XRD) analysis of biochar derived from baobab seeds revealed the absence of well-defined peaks in any phase, as illustrated in Fig. 9. Notably, the XRD patterns showed a pronounced hump in the 18–30 2θ degrees range.
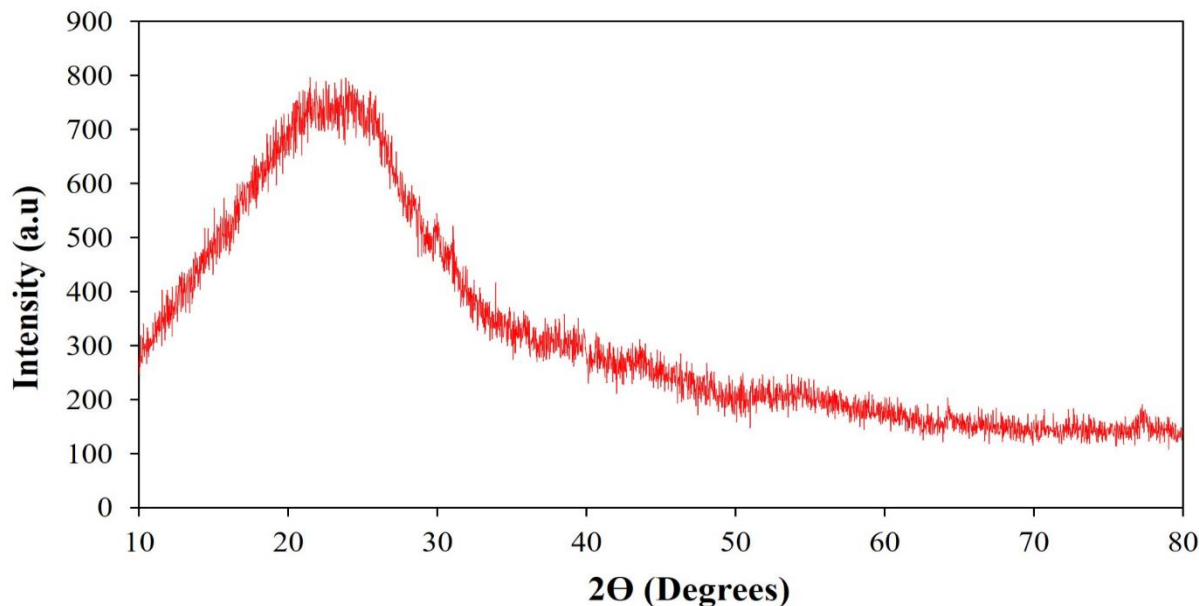
Figure 9:   The X-ray Diffraction (XRD) of the biochar derived from baobab seeds

Brunauer Emmett Teller (BET) Characterization

The results, presented in Fig. 10, illustrate sorption/desorption volume (Va/cm³) of nitrogen gas against relative pressure (p/po). The BET analysis yielded a mean pore diameter of 3.742 nm, a pore volume of 0.402 cm³/g, and a surface area of 1386.704 m²/g. Fig. 11 shows a heterogeneous pore structure in the material. The graph indicates that the pore volume increases significantly as the pore diameter grows, reaching a peak in a specific range, and then shows a noticeable gap before a substantial increase at larger diameters. This trend suggests the presence of a variety of pore sizes, including very small micropores, a dense range of mesopores, and fewer but larger macropores.

52
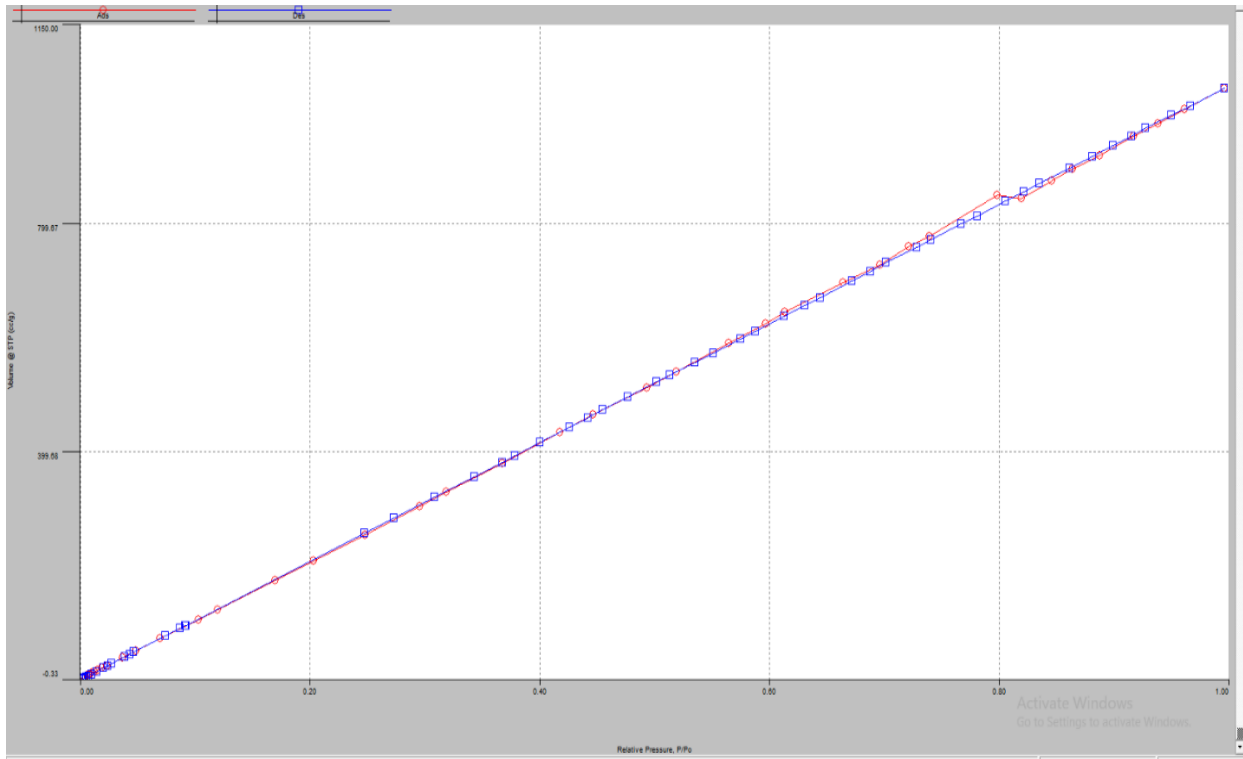
Figure 10: **Adsorption–desorption plot of N2 at 77.35 K for baobab seed-derived biochar**
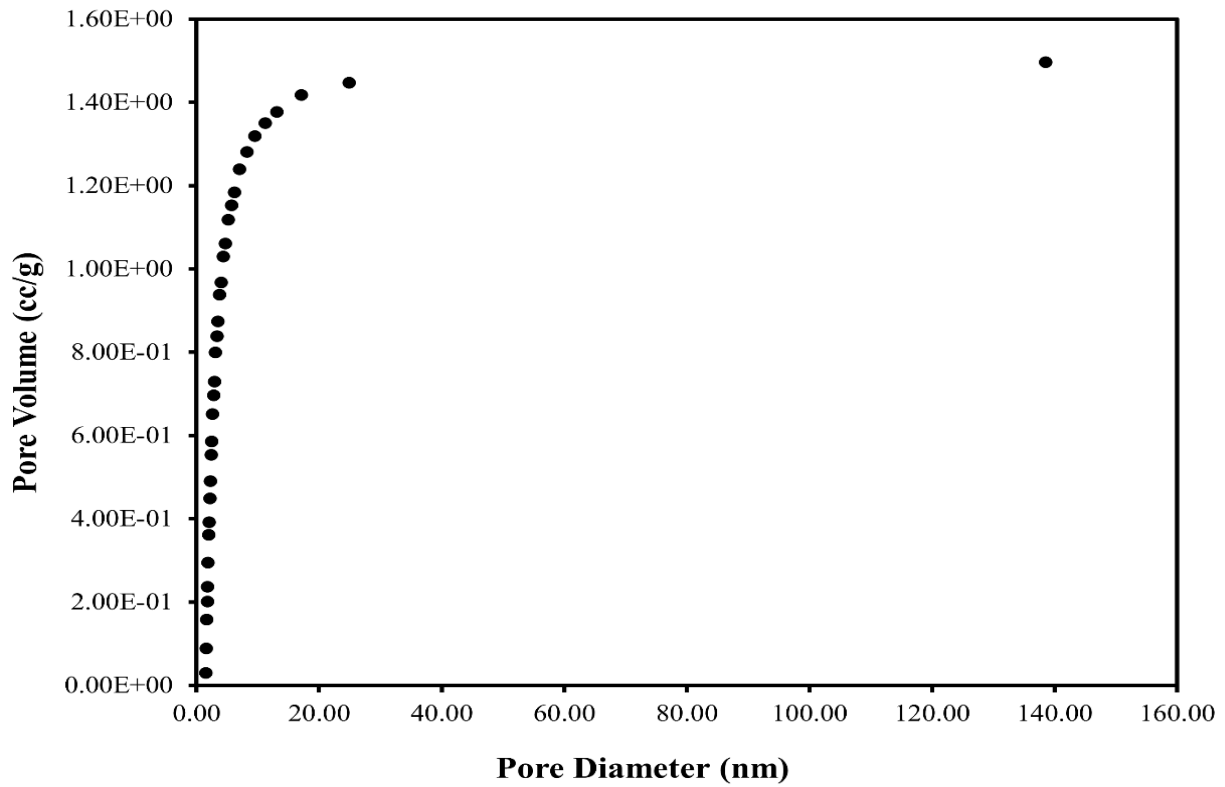
Figure 11: **A graph of pore volume versus radius**

(ii)   Adsorption Kinetics Experiments for Iron Removal

Effect of Adsorbent on Iron Removal at Different pH Levels

The results, as illustrated in Fig. 12, highlighted that the optimal adsorption of iron occurred within the pH range of 5.0–8.0, with the highest adsorption capacity observed at pH 7.0 representing the neutral pH range typical for drinking water. Iron adsorption increased from pH 3 to 8 but decreased with further pH increase (Fig. 12).
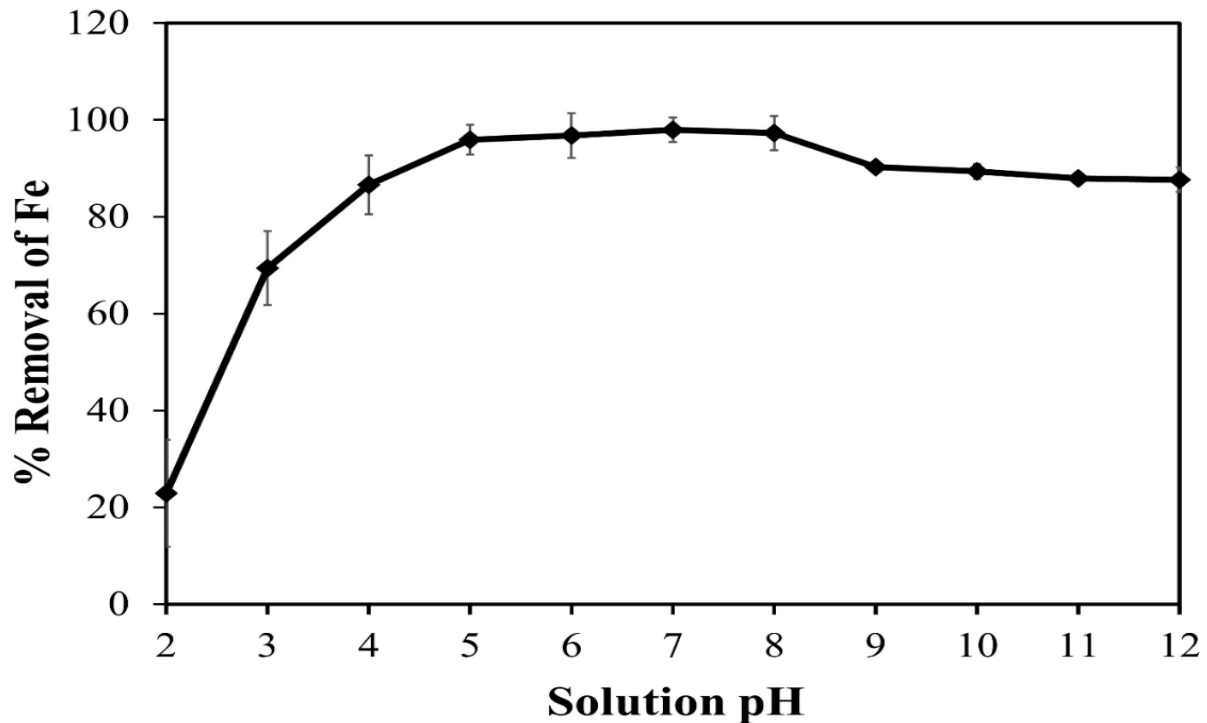
Figure 12:   Effect of pH on the percentage (%) removal of iron

Effect of Contact Time on Iron

The impact of contact time was examined across various contact times, ranging from 20 to 120 minutes, with an initial concentration of 5.88 mg/L in 1000 mL solution flasks. Key operating parameters, including adsorbent dose (3 g/L), agitation speed (120 rpm), room temperature (25±0.5 °C), adsorbent particle size (sieved in 90 μm), and solution pH of 7.0, were kept constant. The results presented in Fig. 13 show that the adsorption capacity increased with increase in contact time up to 120 min. The observed percentage removal of iron by adsorbent exhibited a

54

notable increase with prolonged reaction times, reaching an optimal removal efficiency 87%, within the 120 minutes.
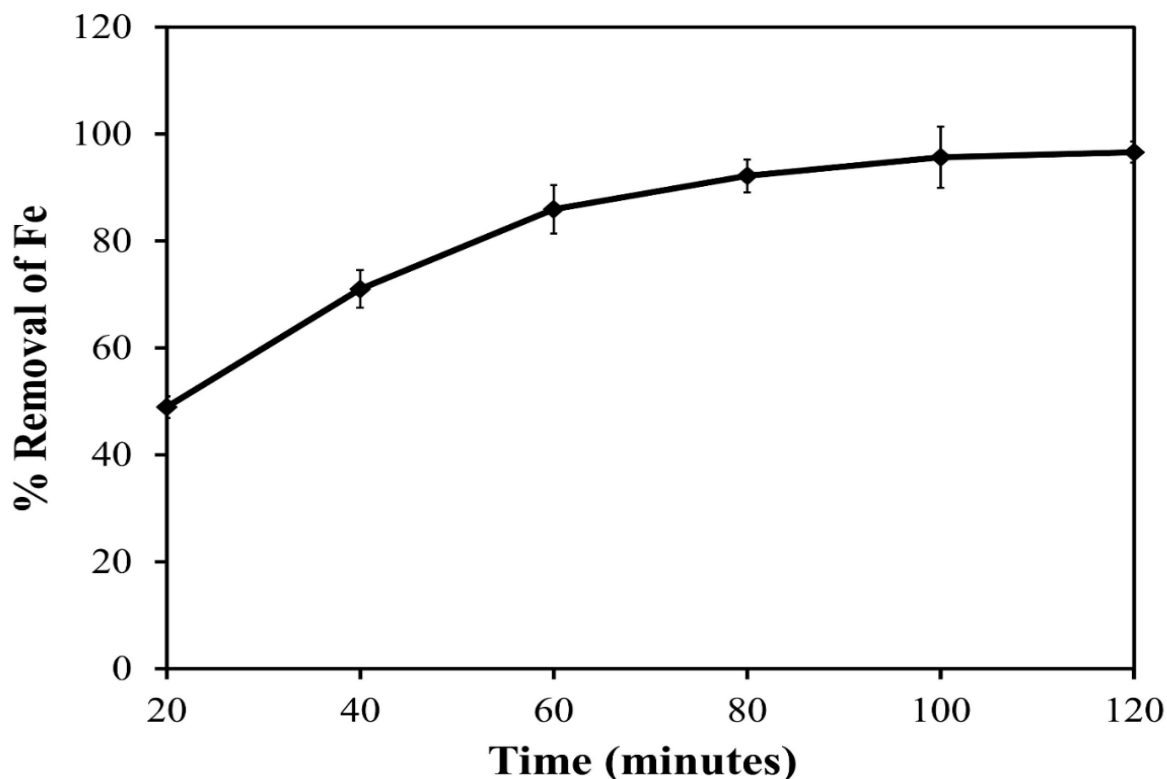
Figure 13:   Effect of contact time with % removal of iron

Effect of Baobab Seeds Biochar Adsorbent Particle Size on Iron Removal

The study investigated the influence of baobab seed-derived biochar adsorbent particle size on the removal of iron from groundwater. Experiments were conducted with varying particle sizes (ranging from 90 to 1000 μm), maintaining constant conditions such as 120 rpm agitation speed, 5.88 mg/L initial iron concentration, 25 ± 0.5 °C solution temperature, pH values of 7, adsorbent dose of 3.0 g and a 120 minutes contact time for removing Fe ions from the groundwater. The experimental results, illustrated in Fig. 14, revealed a decrease in the percentage removal of iron ions by the adsorbent as particle size increased.
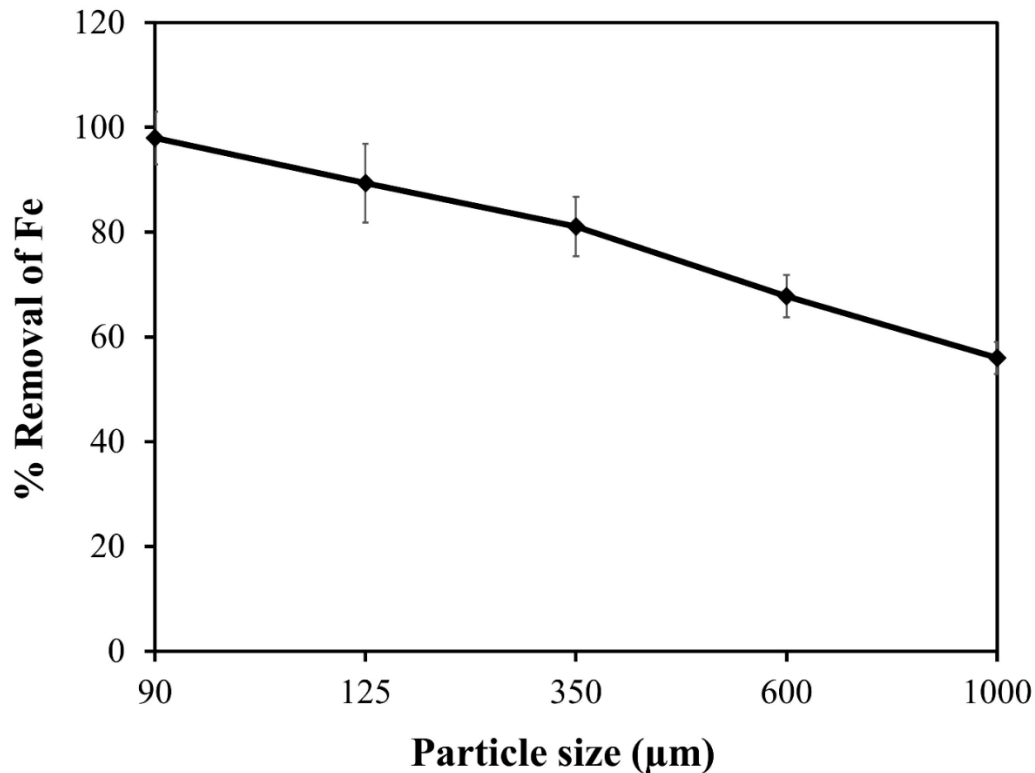
Figure 14: **Effect of particle size with percentage (%) removal of iron.**

Effect of Baobab Seed Biochar Adsorbent Doses on Iron Removal from Water

The baobab seed biochar adsorbent doses on iron removal from water was assessed to see how varying the dosage of a baobab seed-derived biochar (adsorbent). Quantities ranging from 0.3 to 3.9 g/L, while maintaining consistent conditions for agitation speed (120 rpm), room temperature (22 ± 0.5 °C), baobab seed adsorbent particle size (90 μm), initial Fe concentration (5.88 mg/L), and solution pH (7). The percentage removal of iron increased with increasing doses of baobab seed biochar (Fig. 15).
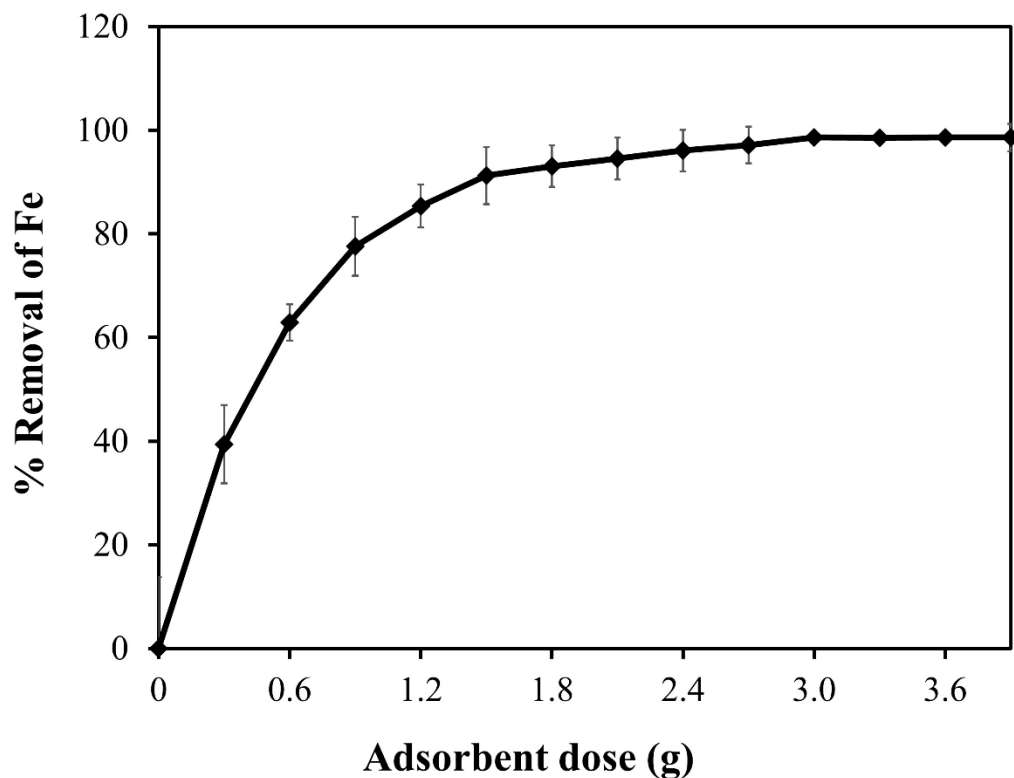
Figure 15:   **Effect of adsorbent dose on iron removal**

Effect of Solution Temperature on Iron Removal from Water

Experimental investigations at varied temperatures such as (20 °C, 25 °C, 30 °C, 35 °C, 40 °C, 45 °C and 50 °C) were performed with consistent conditions for agitation speed (120 rpm), particle size (sieved through 90 μm), initial Fe concentration (5.88 mg/L), and solution pH (7). The results in Fig. 16. indicate an increasing iron removal efficiency with increasing temperatures peaking at 45 °C with a maximum removal efficiency of 98%.
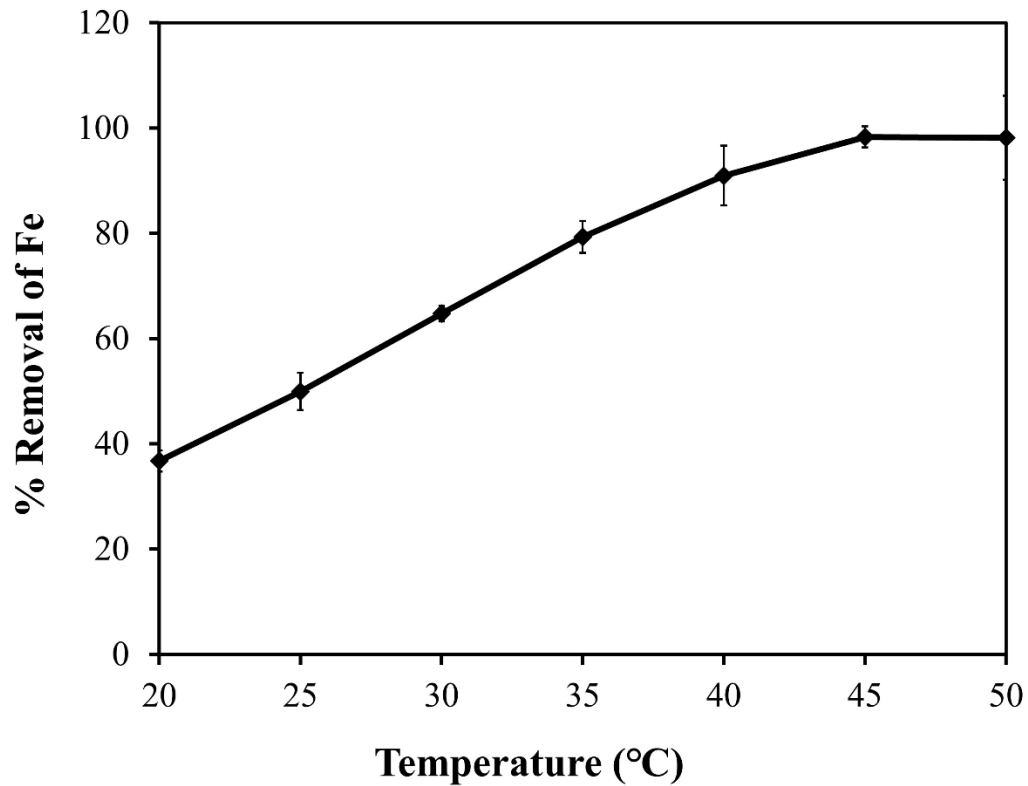
Figure 16: **Effect of solution temperature on iron removal**

Effect of Initial Iron Concentration

The findings depicted in Fig. 17 showed the outcomes of a research analysis that systematically varied the initial concentrations of iron in the range of 2 to 30 mg/L. The results revealed a significant augmentation in the percentage of iron ion removal by the adsorbent derived from baobab seed, ranging impressively from 61% to 94%.
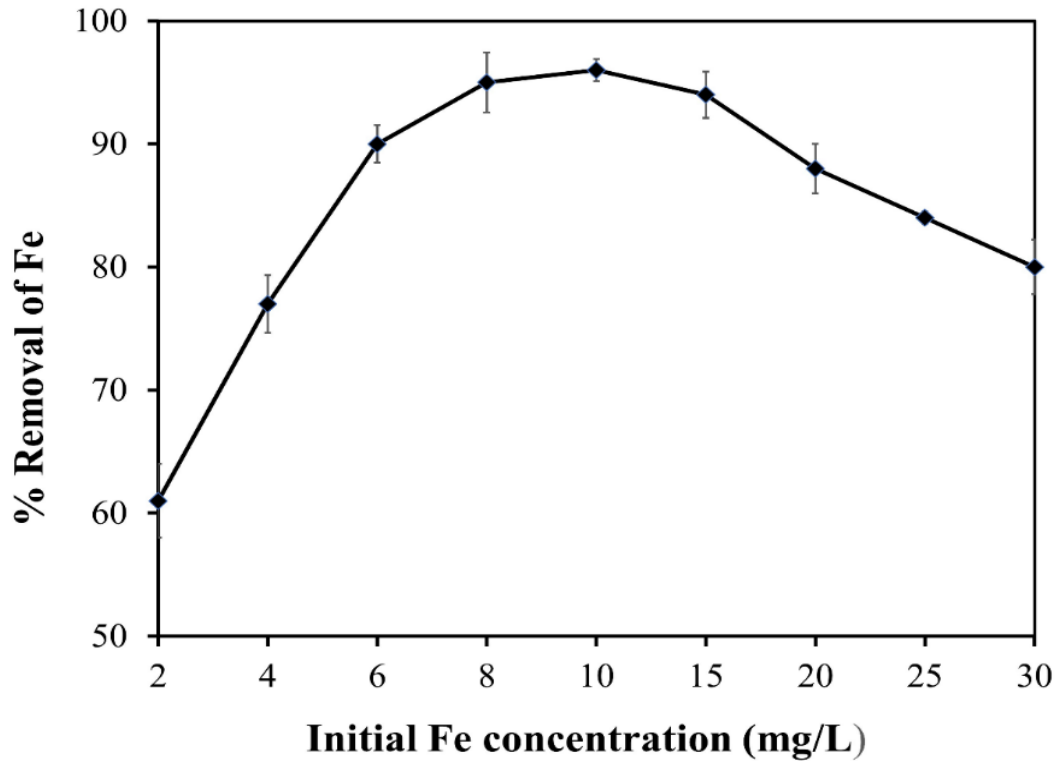
Figure 17:   **Effect of initial concentration on iron removal**

(iii)   **Adsorption Modelling and Kinetics**

Adsorption Isotherm

Fig. 18 shows a plot of C_e/q_e against C_e where the linear form of Langmuir isotherm was applied. The calculated maximum adsorption capacity q_m, adsorption intensity K_L and separation factor R_L are presented Table 13. Fig. 19 presents a plot of $Log q_e$ against $Log c_e$ where the linear Freundlich isotherm was applied. The values of K_f, n and 1/n are reported in Table 13.
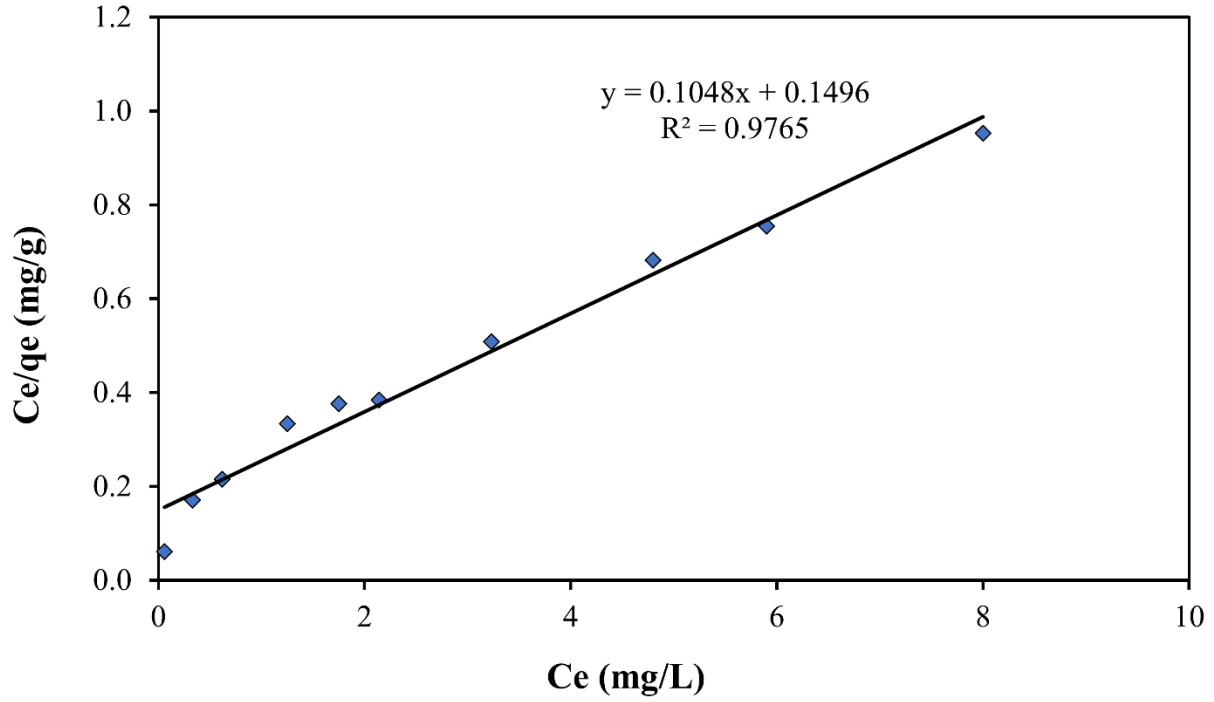
Figure 18: The Langmuir isotherm plot for iron removal using baobab seeds-derived biochar (adsorbent)
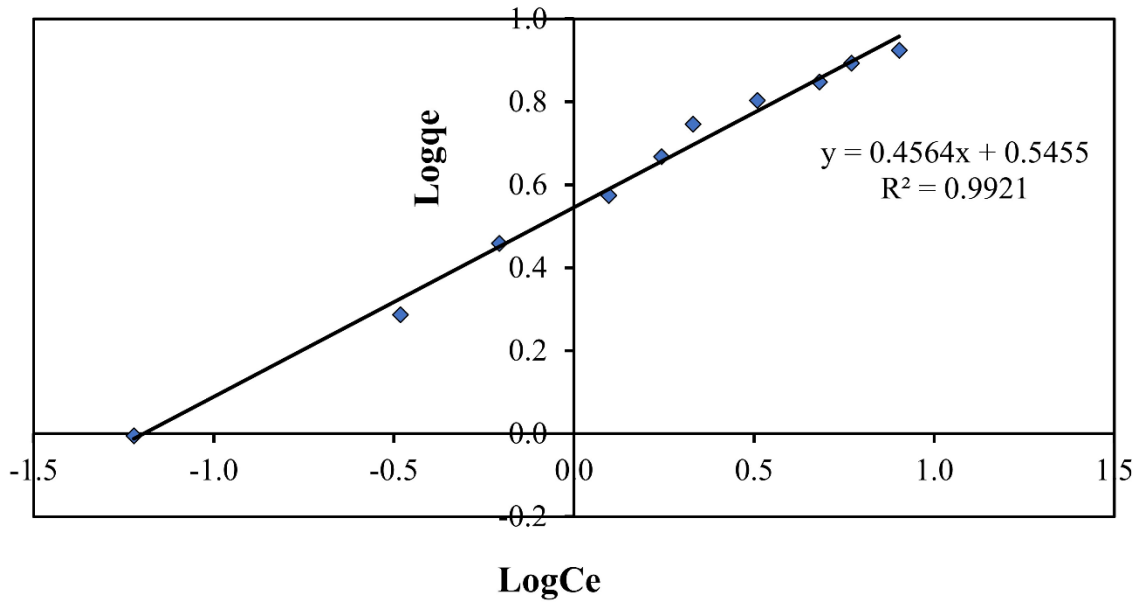
Figure 19: Freundlich isotherm plot for iron removal using baobab seeds-derived biochar (adsorbent)

Table 13:   **Values of the used isotherm parameters at 25 °C**

Isotherm model	Parameter	Values	R^2
Langmuir	q_m	15.8983	
	K_L	0.4205	0.9765
	R_L	0.0013	
Freundlich	K_f	1.72168	
	n	2.1911	0.9921
	1/n	0.4564	

Kinetic Models of Adsorption

The R^2 value from the regression line of the Pseudo 1st and 2nd order kinetic models for the adsorption of Fe were 0.9908 (Fig. 20) and 0.9999 (Fig. 21) respectively. The Pseudo 1st and 2nd order constants obtained from the regression equation were $k_1 = 0.14$ and $k_2 = 0.0232$, respectively (Table 14).
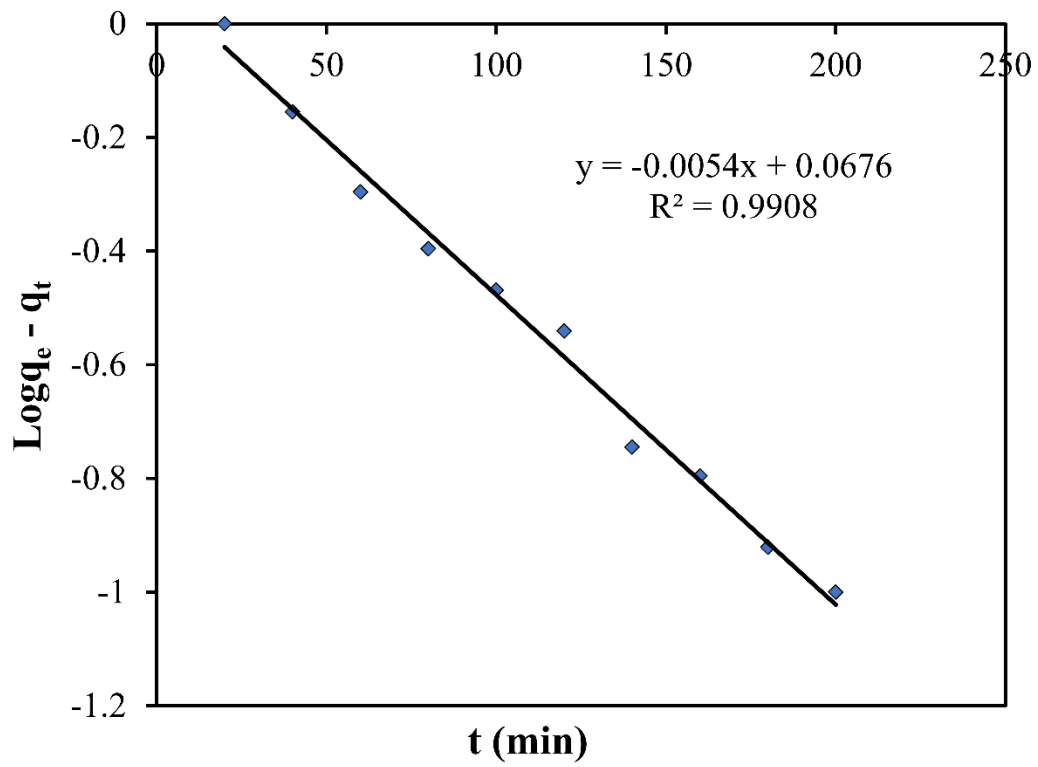
Figure 20: **Pseudo-First Order for iron removal using baobab seeds-derived biochar (adsorbent)**

$$y = 0.1185x + 0.4682$$
$$R^2 = 0.9999$$
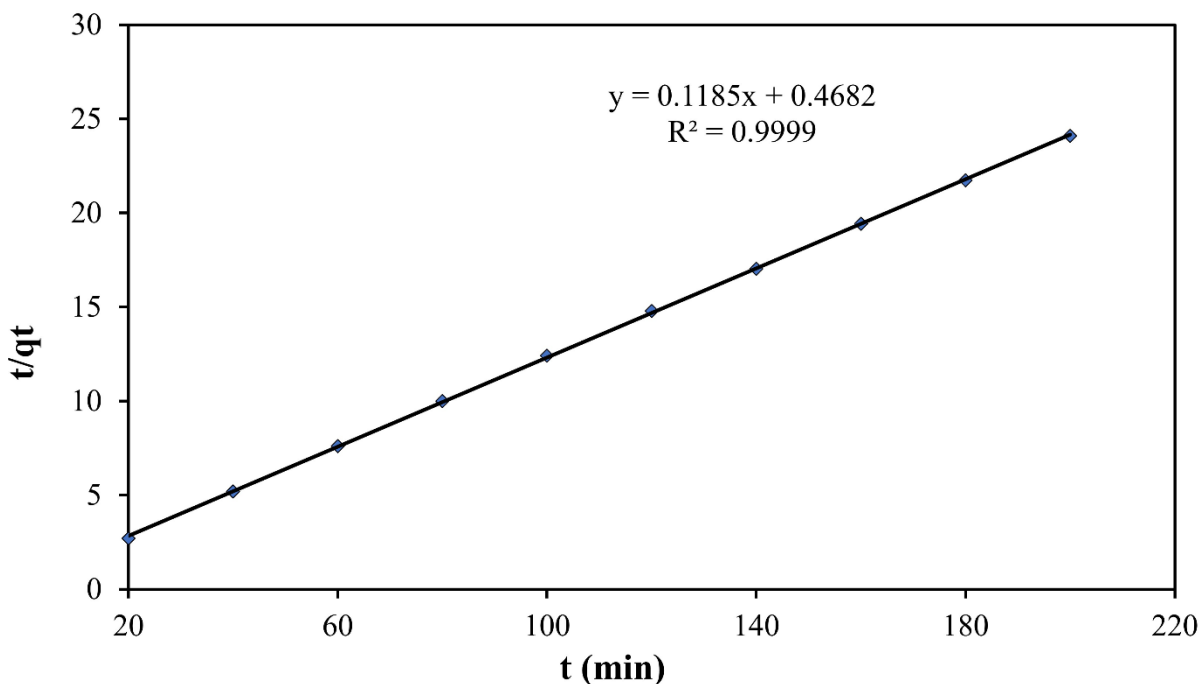
Figure 21: **Pseudo-second order plot of t/q_t against t (min) for iron removal using baobab seeds-derived biochar (adsorbent)**

Table 14: **Parametric values of each kinetic model**

Kinetic model	Parameter	Fitted value
Pseudo-first-order	q_e (exp.) (mg/g)	8.40
	q_e (calc.) (mg/g)	7.82
	K_1 (per min)	0.0138
	R^2	0.9908
Pseudo-second-order	q_e (exp.) (mg/g)	8.40
	q_e (calc.) (mg/g)	8.44
	K_2 (g mg^{-1} min$^{-1)}$)	0.0232
	R^2	0.9999

4.2 Discussion

4.2.1 Physicochemical Parameters and Heavy Metals in Mpanda District

(i) Descriptive Analysis

pH Levels

The pH of groundwater for most of the boreholes were below safe limit (i.e., pH 6.5) given by WHO (2011) and TBS (2018), potentially impacting drinking water quality. Low pH in groundwater can be resulted from organic acids, carbon dioxide, or biogeochemical processes from the decay and leaching of plant materials into groundwater (Adongo *et al*., 2022). The lower pH below 6.5 in water has potential impact on water supply infrastructures such as water pipes because it can lead to corrosion. In addition, it leads to aesthetic problems like a metallic taste impacting drinking water quality (Adongo *et al*., 2022).

Total Dissolved Solids (TDS) and Electrical Conductivity (EC)

The high TDS and EC values observed in the study area is an indication of deterioration of drinking water which mighty lead to consumer dissatisfaction and scaling in household equipment due to dissolved salts and minerals. The elevated TDS and EC in groundwater possibly resulted from dissolved weathered limestone and salts rock materials or the influence of nearby pit latrines in the study area. The findings of this study align with previous studies, for instance Akhtar *et al*. (2014) and Gebresilasie *et al*. (2021) reported TDS in groundwater ranges between 68.2 – 1155.5 mg/L. Additionally, Sankoh *et al*. (2023) reported that, EC ranges between 363 – 2480 µS/cm in the groundwaters.

Dissolved Oxygen (DO)

The low DO in the study area, is an indication of potential oxygen deficiency. Low DO levels in drinking water can cause aesthetic issues including taste and odour and corrosiveness (WHO, 2011).

Temperature

The study also found that, temperature in most of boreholes exceeded WHO limit of 25 °C. The changes in temperature mighty be attributed by seasonal influences and topography (Okpokwasili *et al*., 2013). Also, Gebresilasie *et al*. (2021) reported that the temperature of groundwater investigated in Niger Delta ranged from 24 to 27.9 °C.

Turbidity

Turbidity in most of boreholes in the study area exceeded WHO and TBS maximum recommended values of 5 NTU, potentially indicating pollution which mighty be caused by anthropogenic activities like mining and agriculture. The observed high turbidity values in most sites of the study area are closely related to the presence of Fe and or Mn. The groundwater contains dissolved Fe and Mn in the aquifers, but when comes to exposure to oxygen in the atmosphere, they can oxidize and form precipitates (Adongo *et al*., 2022). Also, Qureshi *et al*. (2021) assessed turbidity in gropundwater in Pakistan and found that, the turbidity ranged from 1.51 to 14. 3 NTU.

Hardness and Chloride

The highest hardness and chloride concentrations above WHO and TBS maximum safe limits was detected at B14 for both seasons. The elevated hardness and chloride concentrations in groundwater could be due to dissolved minerals like calcium and magnesium ions and the nearby pit latrines around the study area. The groundwater samples surpassing 300 mg/L set limit is considered as very hard water. The hardness in the groundwater has negative impact for the infrastructures including soap scum in the pipes and can lead to the blockage of the pipes, deposition of carbonate in the pipes and coating of water tanks (Gebresilasie *et al*., 2021).

Iron (Fe) and Manganese (Mn)

The concentrations of Iron (Fe) and manganese (Mn) in most of boreholes exceeded WHO and TBS allowable limits of 0.3 mg/L and 0.1 mg/L, respectively. Exceeding concentrations of Fe and Mn in the study area mighty be associated with mineral accumulation from rocks in sediment aquifers. These results agree with other researchers for instance Carretero & Kruse (2015) reported that Fe and Mn are abundant in groundwater surrounded by igneous and metamorphic rocks

existing as magnetite and pyrolusite. In addition, high Fe and Mn concentrations can cause staining, bitter taste, and water usability issues (Herschy, 2012).

Lead (Pb)

The accumulation of Pb observed in some boreholes are potentially linked with mining operations which disrupt groundwater system by creating excavations and underground tunnels potentially causing changes in water tables and the movements of contaminants. Exposure to lead in prolonged period, can lead to neurological complications, especially in children (Christine *et al*., 2018). The findings concurred with (Aline Beatrice *et al*., 2019) who observed higher concentrations of Pb in many Edea (Cameroon) boreholes.

Mercury (Hg) and Arsenic (As)

The concentration of mercury (Hg) and Arsenic (As) reported in this study were within the maximum allowable values set by WHO and TBS standards of 6 µg/L and 10 µg/L, respectively.

(ii)   Comparative analysis of water Quality parameters Across Seasons and Groups

The Post Hoc Test results reveal significant variations in water quality parameters between different groups and across the rainy and dry seasons. These variations are crucial for understanding the impact of seasonal changes on water quality and the differential effects on various groups.

Variations Between Groups

In the rainy season, pH levels showed significant differences between multiple group pairs, notably between groups 1 (Ilembo) and 4 (Kakese), groups 2 (Magamba) and 4 (Kakese), groups 1 (Ilembo) and 3 (Sitalike), and groups 2 (Magamba) and 3 (Sitalike). Similarly, in the dry season, significant differences were observed between groups 1 (Ilembo) and 4 (Kakese), groups 1 (Ilembo) and 3 (Sitalike), groups 2 (Magamba) and 4 (Kakese), and groups 2 (Magamba) and 3 (Sitalike). These results suggest that pH levels are highly sensitive to seasonal changes and vary significantly across different groups, possibly due to differences in the geographical or environmental conditions of the boreholes.

Dissolved Oxygen exhibited significant differences in both seasons, though the group pairs differed. In the rainy season, significant differences were noted between groups 3 (Sitalike) and 2 (Magamba), and groups 3 (Sitalike) and 4 (Kakese). In the dry season, significant differences were observed between groups 3 (Sitalike) and 2 (Magamba), and groups 1 (Ilembo) and 2 (Magamba). The variations in DO levels could be attributed to changes in water temperature, organic matter, and microbial activity between seasons.

TDS and EC displayed significant differences only in the rainy season, particularly between groups 4 (Kakese) and 3 (Sitalike), and groups 3 (Sitalike) and 4 (Kakese). The lack of significant differences in the dry season suggests that TDS and EC levels are more stable during this period. Seasonal rainfall likely influences the concentration of dissolved solids and ions, leading to more pronounced differences in the rainy season.

Significant differences in water temperature were observed in the rainy season between groups 1 (Ilembo) and 4 (Kakese), and groups 2 (Magamba) and 4 (Kakese). However, no significant differences were found in the dry season. This pattern indicates that temperature variations are more pronounced during the rainy season, potentially due to increased surface runoff and varying ambient temperatures affecting different boreholes.

Turbidity levels showed significant differences in both seasons, with more group pairs showing differences in the rainy season. Significant differences were found between groups 3 (Sitalike) and 1 (Ilembo), and groups 4 (Kakese) and 1 (Ilembo) in the rainy season, and between groups 3 (Sitalike) and 1 (Ilembo) in the dry season. The increased turbidity during the rainy season could be due to higher sediment load from runoff, whereas dry season differences might be influenced by localized disturbances.

Water hardness varied significantly between groups in both seasons. In the rainy season, differences were significant between groups 4 (Kakese) and 3 (Sitalike), and groups 1 (Ilembo) and 3 (Sitalike), while in the dry season, differences were noted between groups 4 (Kakese) and 3 (Sitalike), and groups 1 (Ilembo) and 3 (Sitalike). These differences indicate that hardness, which is influenced by the presence of calcium and magnesium, fluctuates with seasonal changes in water composition.

Chloride levels showed significant differences in both seasons, with more group pairs showing differences in the dry season. In the rainy season, significant differences were observed between groups 4 (Kakese) and 1 (Ilembo), and groups 4 (Kakese) and 3 (Sitalike). In the dry season, differences were significant between groups 4 (Kakese) and 1 (Ilembo), groups 4 (Kakese) and 3 (Sitalike), and groups 2 (Magamba) and 3 (Sitalike). These findings suggest that chloride concentrations are influenced by both seasonal factors and specific group characteristics, such as local geology or anthropogenic inputs.

Iron levels exhibited significant differences across many group pairs in both seasons. In the rainy season, significant differences were noted between groups 4 (Kakese) and 1 (Ilembo), groups 3 (Sitalike) and 1 (Ilembo), and groups 4 (Kakese) and 3 (Sitalike). In the dry season, differences were observed between groups 4 (Kakese) and 1 (Ilembo), groups 3 (Sitalike) and 1 (Ilembo), and groups 2 (Magamba) and 1 (Ilembo). These differences indicate that iron concentrations are affected by seasonal variations, likely due to changes in water chemistry and redox conditions.

Mercury showed no significant differences in the rainy season but did in the dry season between groups 4 (Kakese) and 1 (Ilembo), groups 3 (Sitalike) and 1 (Ilembo), and groups 2 (Magamba) and 1 (Ilembo). This suggests that mercury levels are more stable during the rainy season but can vary significantly in the dry season, possibly due to changes in water flow and sediment interactions.

Arsenic levels differed significantly in the rainy season between groups 1 (Ilembo) and 3 (Sitalike), and groups 1 (Ilembo) and 2 (Magamba), with no significant differences observed in the dry season. This indicates that arsenic concentrations are more variable during the rainy season, potentially due to increased leaching from soil and rock formations.

Variations Between Seasons

Differences observed in water quality parameters during the rainy and dry seasons particularly high in dry season than rainy season might be attributed to various scientific factors related to hydrology, climate, and environmental conditions.

During the rainy season, increased precipitation leads to greater infiltration of water into the soil, which can recharge groundwater aquifers. This influx of water often dilutes the concentration of

contaminants present in the groundwater, such as metals and nutrients, resulting in lower observed concentrations. In the dry season, reduced rainfall and lower infiltration rates mean less recharge of groundwater, which can concentrate any existing contaminants. With less new water entering the aquifer, the groundwater can become more concentrated with pollutants, leading to higher observed concentrations.

Temperature variations also play a role. During the dry season, higher temperatures can increase evaporation rates and reduce groundwater levels, potentially leading to changes in chemical concentrations. Warmer temperatures can enhance chemical and biological processes that affect water quality, such as increased microbial activity and changes in redox conditions, which can impact the solubility and mobility of certain contaminants. Soil and sediment interactions also play a significant role. During the rainy season, increased water flow can resuspend sediments, releasing contaminants that were previously settled. This can lead to higher turbidity. In the dry season, lower water flow reduces sediment resuspension, allowing contaminants to settle, which can result in lower turbidity.

Furthermore, human activities such as irrigation, industrial use, and groundwater extraction can impact water quality throughout the year. During the dry season, reduced water availability and increased demand for groundwater can exacerbate the effects of contamination, as reduced recharge can limit the natural dilution and dispersion of pollutants.

(iii)   Correlational Analysis

The presence of significant correlations between various physicochemical parameters and heavy metals highlights potential relationships and dependencies within the groundwater system. In the rainy season, strong correlations, such as between pH and Fe, suggesting a potential influence of pH on the solubility and mobility of iron. Similarly, the moderate correlations between parameters like DO and Mn, TDS and Mn, and EC and Mn indicate the potential interactions between dissolved oxygen, total dissolved solids, electrical conductivity, and manganese levels. In the dry season, the observed correlations, particularly the strong correlation between hardness and Mn, suggesting a possible association between water hardness and manganese concentration. Additionally, moderate correlations between parameters like pH and Fe, TDS and Pb, and EC and

Pb, further underscore the complex interplay between various physicochemical factors and heavy metal concentrations in groundwater.

(iv)   Water Quality Index (WQI)

The analysis of the water quality index (WQI) indicated that, no boreholes are within the excellent water category. However, only five boreholes (B04, B06, B08, B10, and B12), both rainy and dry seasons, exhibited good water quality. This suggests their suitability for household use but not for drinking purpose. Conversely, approximately 73.68% of water in the boreholes fall within the poor water and polluted categories implying that, groundwater in the study area is deteriorated and is not fit for drinking due to contaminations by elevated levels of Fe, Mn, and Pb. But, the groundwater in the study area may be suitable for other domestic uses besides drinking. These results concur with other researchers. For instance, Mgbenu & Egbueri (2019) in Umunya District, southeast Nigeria revealed that, large percentage of the sampled groundwater was poor water.

4.2.2   Potential Use of Baobab Seeds to Remove Iron from Groundwater

(i)   Characteristics of Biochar from Baobab Seeds

The morphological characteristics of the adsorbent, baobab seeds-derived biochar, were investigated using a ZEISIS SIGMA 300 VP scanning electron microscope (SEM) coupled with Smart EDX. It was observed that, the baobab seed-derived biochar has deep voids and varied surface morphology, which contribute to a heightened surface area. The heightened surface area provides more sites for the adsorption of iron ions and other contaminants present in groundwater in the study area. These findings are in consistent with prior studies on activated carbon derived from agricultural wastes, which have demonstrated similar structural characteristics favoring adsorption (Siddiq *et al*., 2022). The predominance of carbon in the elemental composition of the biochar observed in EDX (Fig. 8) further supports its suitability for adsorption purposes, as carbonaceous materials are known for their adsorption properties. This study is in consistent with other prior researches on activated carbon from *Jatropha curcas* used for decontamination of water, identified a composition of 93.36% carbon and 6.64% oxygen in the activated carbon (Kalagatur *et al*., 2017; Giordano *et al*., 2003; Tan *et al*., 2021).

Additionally, the X – ray diffraction (XRD) analysis results, revealed the amorphous nature of the biochar material from baobab seeds due to the absence of well-defined peaks in any phase and having a pronounced hump. The amorphous nature is known to possess higher surface areas, which can enhance adsorption capacities, particularly for heavy metal ions such as iron ions (Tan *et al.*, 2021). Also, these observations are consistent with previous studies on activated carbon derived from agricultural wastes, underlining the prevalent amorphous nature in such carbonaceous materials (Bohli *et al.*, 2015; Vunain *et al.*, 2017).

Furthermore, the nitrogen adsorption/desorption isotherm analysis revealed valuable insights into the porosity and surface characteristics of the synthesized carbonaceous adsorbent derived from baobab seeds biochar. The linear relationship observed at low pressure aligns with the expected behavior according to the BET adsorption isotherm theory, indicating monolayer adsorption on a homogeneous surface, which is characteristic of microporous materials (García Blanco *et al.*, 2012). However, the slightly, deviations from linearity during desorption at higher pressures suggest the presence of mesopores in addition to micropores, contributing to surface heterogeneity (García Blanco *et al.*, 2012). The pore distribution graph, begins with very small pore diameters, highlighting the presence of micropores that enhance the material's surface area and are suitable for small molecules. There is a significant increase in pore volume within a specific diameter range, indicating a high concentration of mesopores, which significantly contributes to the material's capacity for medium-sized molecules and overall performance. Following a noticeable gap, a substantial increase at larger diameters reveals the presence of fewer but larger macropores, which could impact the material's ability to accommodate or transport larger molecules or gases. The significant pore volume and surface area further support this, indicating ample active sites available for adsorption reactions (Tan *et al.*, 2021). The previous research study by (Giordano *et al.*, 2003) also reported the linear correlation type for the storage of H_2 in porous materials.

(ii)   Adsorption Kinetics Experiments for Iron Removal

The study results, as illustrated in Fig. 12, investigated the influence of pH on iron ion removal by an adsorbent, revealing a notable and a good trend. Results indicated that iron removal efficiency increased with increasing pH, peaking between 5.0 and 8.0, with optimal performance observed at pH 7.0, typical for neutral drinking water. This increase was attributed to reduced competition of

71

hydrogen ions at higher pH levels, allowing greater iron adsorption. Additionally, at higher pH levels, iron ions may form hydroxide complexes which are more readily adsorbed onto the surface of the adsorbent due to their larger size or altered charge characteristics. However, efficiency declined beyond pH 8, possibly due to saturation of adsorption sites, changes in iron speciation, alterations in the adsorbent's structure, or competing reactions in the solution. A similar trend observed by Priyadarshni *et al.* (2020) who demonstrated an increase in adsorption capacity from pH 2 to 8, followed by a decrease from pH 10 to 12.

The impact of contact time from 20 to 120 minutes was examined while the concentration of iron ions was 5.88 mg/L in 1000 mL solution flasks. The results presented in Fig. 13, indicated an increase in percentage removal of iron ions by the adsorbent with prolonged reaction times, reaching an optimal removal efficiency of 87%, while in the range of 100 and 120 minutes there was a stabilization in removal efficiency. This stabilization is typically resulted from the sufficient interaction of the iron ions onto the surface of the adsorbent maximizing the utilization of available adsorption sites. Subsequently, the extent of iron ion removal remained almost constant with increase in contact time, which is an indicative of saturation of adsorption sites. The same trend was reported by Krishna & Swamy (2012) who showed that the maximum adsorption of biochar occur below 100 min. Fig. 12, revealed a decrease in the percentage removal of iron ions by the adsorbent as particle size increased. This suggests that the larger the particle sizes of adsorbent the less effective of iron ions removal from water. The declined performance of larger particle sizes mighty be attributed to their low surface area per unit mass compared to smaller particle sizes resulting in fewer active sites for adsorption. Additionally, longer diffusion pathways in larger particle sizes can result in slower mass transfer rates, hindering the uptake of iron ions onto the adsorbent surface and reducing removal efficiency. These findings align with the work done by Bayuo *et al.* (2023), suggesting that reducing the particle size enhances metal ions uptake.

Fig. 15 shows the percentage of iron adsorption increased with higher doses of adsorbent. This trend suggests that, higher adsorbent doses resulted into an increased number of active sites for the adsorption of iron ions, allowing for greater removal of iron ions. Additionally, higher doses provide a larger surface area for interaction between the adsorbent and iron ions, facilitating more effective adsorption. The optimal adsorbent dose for achieving maximum iron removal was 3.0 g/L, attaining a removal efficiency of 88.61%. Further increases in adsorbent dose did not yield

significant improvements, indicating the establishment of saturation of the adsorbent's capacity. This observation align with the findings of Verma & Singh (2019), who also reported enhanced iron ion removal with increased adsorbent doses of biochar synthesized from waste plant litter biomass. Higher temperature of 45 °C attained a removal efficiency of 98% (Fig. 16). This might be attributed by the enhanced kinetics of iron ions whereby higher temperatures accelerate the rate of chemical reaction including adsorption processes. Additionally, increased temperature enhances the diffusion of iron ions from the bulk water to the surface of the adsorbent, improving mass transfer rates and facilitating more efficient adsorption. Furthermore, temperature can affect the solubility of iron species in water, with higher temperatures potentially decreasing solubility, leading to increased precipitation and easier removal by the adsorbent. This study is in attribute with the previous study reported by Bayuo *et al*. (2023) who indicated that, optimal removal efficiency of Hg (II) occurred at 45 °C.

The results depicted in Fig. 17 revealed a significant augmentation in the percentage of iron ion removal by the adsorbent derived from baobab seed, ranging impressively from 61% to 94%. At lower initial concentrations (2- 10 mg/L), there is an increase in removal efficiency as more iron ions are adsorbed onto the available active sites on the adsorbent surface. As the initial concentration increases within this range, more iron ions are available to interact with the available active sites, resulting in higher removal efficiency. The results show a peak in removal efficiency at an initial concentration of 10 mg/L, where the percentage removal reaches 94%. This optimal efficiency suggests that the adsorbent is most effective at removing iron ions from the water within this concentration range. At this point, the adsorbent's active sites are sufficiently utilized without being overly saturated, leading to maximum removal efficiency.

(iii) Adsorption Modelling and Kinetics

The analysis of the Langmuir and Freundlich models offers valuable insights into the adsorption process of iron ions onto the biochar surface. The favorable RL value (<1) indicates efficient adsorption, supporting the practical application of the biochar as an adsorbent. The Freundlich model's superiority in fitting the data suggests a heterogeneous adsorption process with varying energies or sites, indicating a multilayer coverage mechanism.

The pseudo-second-order model demonstrated high accuracy ($R^2 > 0.9999$) and provided a calculated q_e value of 8.44 mg/g and is in close agreement with the experimental value of 8.40 mg/g. This suggests that the pseudo-second-order model better describes the adsorption kinetics compared to the pseudo-first-order model. This observation implies that the adsorbate molecules are interacting with multiple sites on the adsorbent surface and that the rate of adsorption is directly proportional to the square of the concentration of the adsorbate. These findings align with the previous study by Verma and Singh (2019) who reported the study results followed the pseudo second order of kinetics.

CHAPTER FIVE

CONCLUSION AND RECOMMENDATIONS

5.1   Conclusion

The study highlights the challenges faced by groundwater in Mpanda district, including acidity and elevated levels of various parameters such as total dissolved solids (TDS), electrical conductivity (EC), temperature, turbidity, hardness, chloride, iron (Fe), manganese (Mn), and lead (Pb). These exceed recommended limits set by WHO and TBS, indicating chemically unsuitable groundwater, particularly during the dry season. Geological factors such as acidic nature, low dissolved oxygen, and higher temperatures contribute to elevated heavy metal levels. For instance, an acidic, low-oxygen, and high-temperature environment can lead to rapid metal release, increased mobility, and higher concentrations of metals. Additionally, Water Quality Index (WQI) analysis reveals that a significant portion of groundwater samples analyzed falls under the poor and polluted water category, making it unsuitable for drinking purposes. Principal Component Analysis (PCA) further confirms the presence of pollution in the groundwater samples.

The study highlights the promising potential of baobab seeds-derived biochar as an effective and sustainable adsorbent for iron removal from groundwater. Through various analytical methods including XRD, SEM-EDX, and BET surface analysis, the physicochemical characteristics of the biochar were thoroughly examined. The XRD spectrum confirmed successful carbonization of baobab seeds into amorphous nature of the biochar, rather than its crystallinity. This amorphous structure is beneficial, as it typically results in a higher surface area. SEM images revealed its porous structure with diverse pore sizes and surface features. The presence of deep voids suggests that the biochar has substantial internal surface areas, which are beneficial for adsorption applications. BET surface analysis further confirmed these findings. The large surface area enhances the biochar's adsorption capacities particularly for heavy metal ions such as iron.

Optimized production conditions resulted in biochar with enhanced adsorption capacity, demonstrated through well-fitted adsorption studies using Freundlich isotherm modeling and the Pseudo second model. These results suggest a heterogeneous adsorption process with multiple adsorption sites, indicating the potential for multilayer coverage. Overall, the study concludes that

75

baobab seed-derived biochar shows great promise as an adsorbent for iron removal from groundwater, making it suitable for water treatment applications.

5.2 Recommendations

Based on the findings of the research study, several recommendations are proposed to address groundwater quality challenges and promote sustainable water management practices. Immediate actions such as water monitoring, treatment, and exploration of alternative water sources are advised in areas with poor water quality classifications. Furthermore, there is a critical need for further research to assess the origins and concentrations of heavy metals over extended periods, alongside geophysical studies focusing on subsurface properties and groundwater quality. Launching awareness campaigns to educate local communities about contaminated groundwater risks and promoting water conservation practices is essential for mitigating contamination sources. Advocating for stricter regulations and enforcement of environmental standards, particularly in industrial, mining, and agricultural sectors, is crucial to prevent further groundwater contamination. Allocating resources for long-term research and monitoring programs will provide valuable data for identifying contamination sources and implementing targeted remediation efforts, ultimately ensuring better management and protection of groundwater resources.

Regarding the effectiveness of baobab seed-derived biochar, this study has demonstrated its potential in mitigating groundwater contamination. It is highly recommended to focus on applied research to scale up the use of this biochar. Developing and implementing biochar-based filters for treating water in Mpanda boreholes could offer a sustainable and effective solution for improving water quality. Future research should focus on optimizing the production process, evaluating the lifespan and long-term performance of the adsorbents, and assessing the economic feasibility and accessibility of these filters for local communities.

Moreover, while the study achieved a maximum iron removal efficiency of 87%, further research is advised to explore methods such as activated carbon for enhancing this performance. Additionally, expanding research to investigate the biochar's effectiveness in removing other contaminants such as manganese and lead, and potentially harmful organic compounds, will provide a more comprehensive understanding of its broad-spectrum water purification capabilities. This approach will not only enhance the applicability of baobab seed-derived biochar but also contribute to ensuring safer drinking water by addressing multiple contaminants simultaneously.

REFERENCES

Abegaz, M. T., & Midekssa, M. J. (2021). Quality and Safety of Rural Community Drinking Water Sources in Guto Gida District, Oromia, Ethiopia. *Journal of Environmental and Public Health*, *2021*. https://doi.org/10.1155/2021/5568375

Adongo, M. J., Makokha, M. K., Obando, J. A., & Ochieng, J. O. (2022). Seasonal Variation in Physicochemical Properties of Groundwater: A Case Study of Kamiti-Marengeta Subcatchment Kiambu, Kenya. *Journal of Water Resource and Protection*, *14*(02), 72–85. https://doi.org/10.4236/jwarp.2022.142005

Agbaka, J. I. (2020). African baobab: Its Role in Enhancing Nutrition, Health, and the Environment. In *Trees, Forests and People*. Elsevier B.V. https://doi.org/10.1016/j.tfp.2020.100043

Akhtar, M. M., Tang, Z., & Mohamadi, B. (2014). Contamination potential assessment of potable groundwater in Lahore, Pakistan. *Polish Journal of Environmental Studies*, *23*(6), 1905–1916. https://www.pjoes.com/ Contamination - Potential - Assessment - of - Potable - r - n Groundwater-in-Lahore-Pakistan, 89385,0,2. html

Akintola, O. O., Aderounmu, A. F., Abiola, I. O., & Bodede, I. A. (2019). Remediation potential of Baobab (*Adansonia digitata L.*) Seedlings grown in sewage sludge contaminated by Heavy Metals. *Journal of Applied Sciences and Environmental Management*, *23*(9), 1691. https://doi.org/10.4314/jasem.v23i9.14

Al-Fartusie, F. S., & Mohssan, S. N. (2017). Essential Trace Elements and Their Vital Roles in Human Body. *Indian Journal of Advances in Chemical Science*, *5*, 127–136. https://doi.org/10.22607/IJACS.2017.503003

Al-Ghouti, M. A., & Da'ana, D. A. (2020). Guidelines for the use and interpretation of adsorption isotherm models: A review. *Journal of Hazardous Materials*, *393*(November 2019), 122383. https://doi.org/10.1016/j.jhazmat.2020.122383

Alam, M. W., Pandey, P., Khan, F., Souayeh, B., & Farhan, M. (2020). Study to investigate the potential of combined extract of leaves and seeds of moringa oleifera in groundwater

purification. *International Journal of Environmental Research and Public Health*, *17*(20), 1–13. https://doi.org/10.3390/ijerph17207468

Aline Beatrice, N., Karen Brell, M., Aboubakar, A., Youtha Armelle Stéphanie, Y., Yaka Diane Armelle, M., Zing Bertrand, Z., Yong Nina Nindum, S., Anselme Crépin, M., & Mewouo Yvette Clarisse, M. (2019). Assessment of Physicochemical and Heavy Metal Properties of Groundwater in Edéa (Cameroon). *American Journal of Water Resources*, *7*(1), 1–10. https://doi.org/10.12691/ajwr-7-1-1

APHA. (2012). *Standard Methods for the Examination of Water and Wastewater*. American Public Health Association. USA, 1496. https: //beta-static. fishersci. com/content/ dam/ fishersci/ en_US/documents/programs/scientific/technical-documents/white-papers/apha - water - testing - standard - methods - introduction - white - paper. pdf

Assogbadjo, A. E., Chadare, F. J., Manda, L., & Sinsin, B. (2021). A 20-Year Journey Through an Orphan African Baobab (Adansonia digitata L.) Towards Improved Food and Nutrition Security in Africa. *Frontiers in Sustainable Food Systems*, *5*(December), 1–17. https://doi.org/10.3389/fsufs.2021.675382

Bayuo, J., Rwiza, M. J., & Mtei, K. M. (2023a). Adsorption and desorption ability of divalent mercury from an interactive bicomponent sorption system using hybrid granular activated carbon. *Environmental Monitoring and Assessment*, *195*(8). https://doi.org/10.1007/s10661-023-11540-y

Bayuo, J., Rwiza, M. J., & Mtei, K. M. (2023b). Modeling and optimization of trivalent arsenic removal from wastewater using activated carbon produced from maize plant biomass: a multivariate experimental design approach. *Biomass Conversion and Biorefinery*, *June*. https://doi.org/10.1007/s13399-023-04494-1

bin Jusoh, A., Cheng, W. H., Low, W. M., Nora'aini, A., & Megat Mohd Noor, M. J. (2005). Study on the removal of iron and manganese in groundwater by granular activated carbon. *Desalination*, *182*(1–3), 347–353. https://doi.org/10.1016/j.desal.2005.03.022

Bohli, T., Ouederni, A., Fiol, N., & Villaescusa, I. (2015). Evaluation of an activated carbon from

olive stones used as an adsorbent for heavy metal removal from aqueous phases. *Comptes Rendus Chimie*, *18*(1), 88–99. https://doi.org/10.1016/j.crci.2014.05.009

Bora, A. J., & Dutta, R. K. (2019). Removal of metals (Pb, Cd, Cu, Cr, Ni, and Co)from drinking water by oxidation-coagulation-absorption at optimized pH. *Journal of Water Process Engineering*, *31*(April), 100839. https://doi.org/10.1016/j.jwpe.2019.100839

Boulton, A. J. (2000). River ecosystem health down under: Assessing ecological condition in riverine groundwater zones in Australia. *Ecosystem Health*, *6*(2), 108–118. https://doi.org/10.1046/j.1526-0992.2000.00011.x

Carrard, N., Foster, T., & Willetts, J. (2019). Groundwater as a source of drinking water in southeast Asia and the Pacific: A multi-country review of current reliance and resource concerns. *Water (Switzerland)*, *11*(8). https://doi.org/10.3390/w11081605

Carretero, S., & Kruse, E. (2015). Iron and manganese content in groundwater on the northeastern coast of the Buenos Aires Province, Argentina. *Environmental Earth Sciences*, *73*(5), 1983–1995. https://doi.org/10.1007/s12665-014-3546-5

Chandler, J. (1989). Iron and manganese. *Water Well Journal*, *43*(3), 40–42. https: //doi. org/10. 1201/ 9780429155833-10

Christine, A. A., Kibet, J. K., Kiprop, A. K., & Were, M. L. (2018). The assessment of bore-hole water quality of Kakamega County, Kenya. *Applied Water Science*, *8*(1), 1–8. https://doi.org/10.1007/s13201-018-0688-8

Civardi, J., & Tompeck, M. (2015). Overview of Treatment Technologies. *Iron and Manganese Removal Handbook*, 35–46. https: //www. eawag. ch /fileadmin /Domain1 /Abteilungen /sandec /publikationen/EWM/Book/FSM_Ch05_Treatment_Technologies.pdf

Danielopol, D. A. N. L., Griebler, C., & Gunatilaka, A. (2003). *Present _ state _ and _ future _ prospects_for_g*. *30*(2). https://doi.org/10.1017/S0376892903000

Edogbanya, O., Abolude, D., Adelanwa, M., & Ocholi, O. (2016). The Efficacy of the Seeds of Adansonia digitata L. as a Biocoagulant and Disinfectant in Water Purification. *Journal of*

Earth, Environment and Health Sciences, *2*(3), 122. https: //doi. org/ 10.4103/ 2423-7752.199289

Edori, O., & Kpee, F. (2016). Physicochemical and Heavy Metal Assessment of Water Samples from Boreholes near Some Abattoirs in Port Harcourt, Rivers State, Nigeria. *American Chemical Science Journal*, *14*(3), 1–8. https://doi.org/10.9734/acsj/2016/22525

El Azher, N., Gourich, B., Vial, C., Soulami, M. B., & Ziyad, M. (2008). Study of ferrous iron oxidation in Morocco drinking water in an airlift reactor. *Chemical Engineering and Processing: Process Intensification*, *47*(9–10), 1877–1886. https:// doi. org / 10.1016/ j. cep. 2007.10.013

Elisante, E., & Muzuka, A. N. N. (2017). Occurrence of nitrate in Tanzanian groundwater aquifers: A review. *Applied Water Science*, *7*(1), 71–87. https://doi.org/10.1007/s13201-015-0269-z

Elwakeel, K. Z., El-Sayed, G. O., & Abo El-Nassr, S. M. (2015). Removal of ferrous and manganous from water by activated carbon obtained from sugarcane bagasse. *Desalination and Water Treatment*, *55*(2), 471–483. https://doi.org/10.1080/19443994.2014.919606

Mussa, K. R., Mjemah, I. C. & Walraevens, K. (2019). Quantification of Groundwater Exploitation and Assessment of Water Quality Risk Perception in the the Dar Es Salaam Quaternary Aquifer, Tanzania. *Water*, 11(12), 2552; https://doi.org/10.3390/w11122552

Fraga, C. G. (2005). Relevance, essentiality and toxicity of trace elements in human health. *Molecular Aspects of Medicine*, *26*(4-5 SPEC. ISS.), 235–244. https:// doi. org/ 10. 1016/ j. mam.2005.07.013

García Blanco, A. A., Vallone, A. F., Gil, A., & Sapag, K. (2012). A comparative study of various microporous materials to store hydrogen by physical adsorption. *International Journal of Hydrogen Energy*, *37*(19), 14870–14880. https://doi.org/10.1016/j.ijhydene.2012.01.166

Gebauer, J., Adam, Y. O., Sanchez, A. C., Darr, D., Eltahir, M. E. S., Fadl, K. E. M., Fernsebner, G., Frei, M., Habte, T. Y., Hammer, K., Hunsche, M., Johnson, H., Kordofani, M., Krawinkel, M., Kugler, F., Luedeling, E., Mahmoud, T. E., Maina, A., Mithöfer, D., … Kehlenbeck, K. (2016). Africa's wooden elephant: the baobab tree (Adansonia digitata L.) in Sudan and

Kenya: a review. *Genetic Resources and Crop Evolution*, *63*(3), 377–399. https: // doi. org/ 10. 1007/s10722-015-0360-1

Gebresilasie, K. G., Berhe, G. G., Tesfay, A. H., & Gebre, S. E. (2021). *Assessment of Some Physicochemical Parameters and Heavy Metals in Hand-Dug Well Water Samples of Kafta Humera Woreda , Tigray , Ethiopia*. *2021*.

Giordano, R., Serp, P., Kalck, P., Kihn, Y., Schreiber, J., Marhic, C., & Duvail, J. L. (2003). Preparation of rhodium catalysts supported on carbon nanotubes by a surface mediated organometallic reaction. *European Journal of Inorganic Chemistry*, *4*, 610–617. https://doi.org/10.1002/ejic.200390083

Haouti, R. El, Anfar, Z., Et-Taleb, S., Benafqir, M., Lhanafi, S., & Alem, N. El. (2018). Removal of heavy metals and organic pollutants by a sand rich in iron oxide. *Euro-Mediterranean Journal for Environmental Integration*, *3*(1). https://doi.org/10.1007/s41207-018-0058-9

Hashim, M. A., Mukhopadhyay, S., Sahu, J. N., & Sengupta, B. (2011). Remediation technologies for heavy metal contaminated groundwater. *Journal of Environmental Management*, *92*(10), 2355–2388. https://doi.org/10.1016/j.jenvman.2011.06.009

Herschy, R. W. (2012). Water quality for drinking: WHO guidelines. *Encyclopedia of Earth Sciences Series*, 876–883. https://doi.org/10.1007/978-1-4020-4410-6_184

Hossain, D., Islam, M., Sultana, N., & Tusher, T. (2015). Assessment of Iron Contamination in Groundwater at Tangail Municipality, Bangladesh. *Journal of Environmental Science and Natural Resources*, *6*(1), 117–121. https://doi.org/10.3329/jesnr.v6i1.22051

Isaeva, M., & Castro, N. M. (2011). Water Treatment for the Removal of Iron and Manganese. *Bachelors Degree Project*. Margarita Isaeva & Natasha Montes Castro. https://www.diva-portal.org/smash/get/diva2:460329/FULLTEXT01.pdf

Ishaque, F., & Ritu, S. (2016). Evaluation of Low Cost Filter Column to Remove Iron from Evaluation of Low Cost Filter Column to Remove Iron from drinking water. *Journal of the Sylhet Agricultural University, 3*(2):263-270. https: //jsau.sau.ac.bd/wp-content/ uploads /2017/12/14. - ID-2017 - 15-V3N2 - Altaf. pdf

Jailos, P., Chimtali, P. J., & Vunain, E. (2021). Assessment of Groundwater Quality in Areas Surrounding Thundulu Phosphate Mine, Phalombe District, Malawi. *Tanzania Journal of Science*, *47*(3), 1310–1321. https://doi.org/10.4314/tjs.v47i3.38

Jha, M. K., Shekhar, A., & Jenifer, M. A. (2020). Assessing groundwater quality for drinking water supply using hybrid fuzzy-GIS-based water quality index. *Water Research*, *179*, 115867. https://doi.org/10.1016/j.watres.2020.115867

Kalagatur, N. K., Karthick, K., Allen, J. A., Ghosh, O. S. N., Chandranayaka, S., Gupta, V. K., Krishna, K., & Mudili, V. (2017). Application of activated carbon derived from seed shells of Jatropha curcas for decontamination of zearalenone mycotoxin. *Frontiers in Pharmacology*, *8*(OCT). https://doi.org/10.3389/fphar.2017.00760

Kew, M. C. (2014). Hepatic iron overload and hepatocellular carcinoma. *Liver Cancer*, *3*(1), 31–40. https://doi.org/10.1159/000343856

Khatri, N., Tyagi, S., & Rawtani, D. (2017). Recent strategies for the removal of iron from water: A review. *Journal of Water Process Engineering*, *19*(13), 291 – 304. https: //doi. org/ 10. 1016/j.jwpe.2017.08.015

Knowles, R., & Wareing, J. (2022). Population Distribution. *Economic and Social Geography*, *1B*, 51–63. https://doi.org/10.1016/b978-0-7506-0922-7.50010-6

Kostrzewa, R. M. (2014). Handbook of neurotoxicity. In *Handbook of Neurotoxicity* (Vols. 1–3, Issue May 2015). https://doi.org/10.1007/978-1-4614-5836-4

Krishna, R. H., & Swamy, A. V. V. S. (2012). Physico-Chemical Key Parameters, Langmuir and Freundlich isotherm and Lagergren Rate Constant Studies on the removal of divalent nickel from the aqueous solutions onto powder of calcined brick. *International Journal of Engineering Research and Development*, *4*(1), 29–38.

Latif, A., Sheng, D., Sun, K., Si, Y., Azeem, M., Abbas, A., & Bilal, M. (2020). Remediation of heavy metals polluted environment using Fe-based nanoparticles: Mechanisms, influencing

factors, and environmental implications. *Environmental Pollution*, *264*, 114728. https://doi.org/10.1016/j.envpol.2020.114728

Le, N. L., & Nunes, S. P. (2016). Materials and membrane technologies for water and energy sustainability. *Sustainable Materials and Technologies*, *7*, 1 – 28. https:// doi. org /10. 1016/ j.susmat.2016.02.001

Liu, C., Wang, W., Wang, H., Zhu, C., & Ren, B. (2023). A Review on Removal of Iron Impurities from Quartz Mineral. *Minerals*, *13*(9), 2806–2813. https://doi.org/10.3390/min13091128

Mcpeak, J. F., & Aronovitch, H. L. (1983). Iron in water and processes for its removal. *21st Annual Liberty Bell Corrosion Course*. Philadelphia, Pennsylvania. file: //C:/ Users/ Hp /Desktop /Iron__in_water.pdf

Mgbenu, C. N., & Egbueri, J. C. (2019). The hydrogeochemical signatures, quality indices and health risk assessment of water resources in Umunya district, southeast Nigeria. *Applied Water Science*, *9*(1), 1–19. https://doi.org/10.1007/s13201-019-0900-5

Michel, M. M., Reczek, L., Papciak, D., Wlodarczyk-Makula, M., Siwiec, T., & Trach, Y. (2020). Mineral materials coated with and consisting of MnOx - Characteristics and application of filter media for groundwater treatment: A Review. *Materials*, *13*(10), 1–35. https://doi.org/10.3390/ma13102232

Mihale, M. J. (2022). Water Quality Evaluation in Costal Rivers of Tanzania Using Water Quality Index. *Open Science Journal*, *March*, 1–18.

Mutula Joseph, J. (2016). *Iron Removal From Borehole Water: a Case Study of Kiambu Town*.

Nisar, N., Koul, B., & Koul, B. (2020). Application of Moringa Oleifera Lam. Seeds in Wastewater Treatment. *Plant Archives*, *21*(supplement), 2408 – 2417. https: //doi. org /10.51470 /plantarchives.2021.v21.s1.393

Noether, G. E. (1992). *Introduction to Wilcoxon (1945) Individual Comparisons by Ranking Methods. 1945*, 191–195. https://doi.org/10.1007/978-1-4612-4380-9_15

Okpokwasili, G. C., Douglas, S. I., & Inengite, A. K. (2013). Seasonal variations of some physicochemical parameters of groundwater in crude oil flow stations. *Journal of Environmental Science and Water Resources*, *2*(January), 16–21.

Palmucci, W., Rusi, S., & Di Curzio, D. (2016). Mobilisation processes responsible for iron and manganese contamination of groundwater in Central Adriatic Italy. *Environmental Science and Pollution Research*, *23*(12), 11790–11805. https://doi.org/10.1007/s11356-016-6371-4

Pantaleo, P. A., Komakech, H. C., Mtei, K. M., & Njau, K. N. (2018). Contamination of groundwater sources in emerging African towns: The case of Babati town, Tanzania. *Water Practice and Technology*, *13*(4), 980–990. https://doi.org/10.2166/wpt.2018.104

Pascu, D. E., Neagu, M., Traistaru, G. A., Nechifor, A. C., & Miron, A. R. (2016). Iron and manganese removal from drinking water. *Journal of Electrochemical Science and Engineering*, *6*(1), 47–55. https://doi.org/10.5599/jese.244

Patra, J. M., Panda, S. S., & Dhal, N. K. (2017). Biochar as a low-cost adsorbent for heavy metal removal: A review. *International Journal of Research in Biosciences*, *6*(1), 1–7. http://www.ijrbs.in

Pepper, D. (1980). Basics of Reverse Osmosis. *Symposium Papers - Institution of Chemical Engineers, North Western Branch*, 1–16.

Priyadarshni, N., Nath, P., Nagahanumaiah, & Chanda, N. (2020). Sustainable removal of arsenate, arsenite and bacterial contamination from water using biochar stabilized iron and copper oxide nanoparticles and associated mechanism of the remediation process. *Journal of Water Process Engineering*, *37*(July), 101495. https://doi.org/10.1016/j.jwpe.2020.101495

Qin, S., Ma, F., Huang, P., & Yang, J. (2009). Fe (II) and Mn (II) removal from drilled well water: A case study from a biological treatment unit in Harbin. *Desalination*, *245*(1–3), 183–193. https://doi.org/10.1016/j.desal.2008.04.048

Qureshi, S. S., Channa, A., Memon, S. A., Khan, Q., Jamali, G. A., Panhwar, A., & Saleh, T. A. (2021). Assessment of physicochemical characteristics in groundwater quality parameters. *Environmental Technology and Innovation*, *24*, 101877. https: // doi. org /10. 1016/j.eti.2021.

101877

Rader, L. (2009). Tech Brief - How To Operate and Maintain Manganese Greensand Treatment Units. *On Tap NESC*. https://files.knowyourh2o.com/Waterlibrary/privatewell/greensand.pdf

Rahim, A. A., & Garba, Z. N. (2016). Efficient adsorption of 4-Chloroguiacol from aqueous solution using optimal activated carbon: Equilibrium isotherms and kinetics modeling. *Journal of the Association of Arab Universities for Basic and Applied Sciences*, *21*, 17–23. https://doi.org/10.1016/j.jaubas.2015.09.001

Rahman, M. M., Islam, M. A., Bodrud-Doza, M., Muhib, M. I., Zahid, A., Shammi, M., Tareq, S. M., & Kurasaki, M. (2018). Spatio-Temporal Assessment of Groundwater Quality and Human Health Risk: A Case Study in Gopalganj, Bangladesh. *Exposure and Health*, *10*(3), 167–188. https://doi.org/10.1007/s12403-017-0253-y

Rahmanian, N., Hajar, S., Ali, B., Homayoonfard, M., Ali, N. J., Rehan, M., Sadef, Y., & Nizami, A. S. (2015). Analysis of physiochemical parameters to evaluate the drinking water quality in the State of Perak, Malaysia. *Journal of Chemistry*, *2015*(Cd), 10-19. https://doi.org/10.1155/2015/716125

Rao, K. S., Anand, S., & Venkateswarlu, P. (2010). Psidium guvajava L leaf powder - A potential low-cost biosorbent for the removal of cadmium(II) ions from wastewater. *Adsorption Science and Technology*, *28*(2), 163–178. https://doi.org/10.1260/0263-6174.28.2.163

Reta, G. L., Dong, X., Su, B., Hu, X., Bo, H., Wan, H., Liu, J., Li, Y., Peng, T., Ma, H., Wang, K., & Xu, S. (2019). The Influence of Large Scale Phosphate Mining on the Water Quality of the Huangbaihe River Basin in China: Dominant Pollutants and Spatial Distributions. *Mine Water and the Environment*, *38*(2), 366–377. https://doi.org/10.1007/s10230-019-00604-6

Rushdi, M. I., Basak, R., Das, P., Ahamed, T., & Bhattacharjee, S. (2023). Assessing the health risks associated with elevated manganese and iron in groundwater in Sreemangal and Moulvibazar Sadar, Bangladesh. *Journal of Hazardous Materials Advances*, *10*(March), 100287. https://doi.org/10.1016/j.hazadv.2023.100287

Rwiza, M. J., Kleinke, M., & Kim, K. W. (2020). A study on Pb removal kinetics using modified

agricultural wastes from Tanzania. *SN Applied Sciences*, *2*(11), 1–12. https: //doi. org/10. 1007/s42452 - 020-03743-6

Rwiza, M. J., Oh, S. Y., Kim, K. W., & Kim, S. D. (2018). Comparative sorption isotherms and removal studies for Pb(II) by physical and thermochemical modification of low-cost agro-wastes from Tanzania. *Chemosphere*, *195*(Ii), 135–145. https: //doi. org/10. 1016/j. chemosphere.2017.12.043

Salvador, G. A., Uranga, R. M., & Giusto, N. M. (2011). Iron and mechanisms of neurotoxicity. *International Journal of Alzheimer's Disease*, *2011*. https://doi.org/10.4061/2011/720658

Sankoh, A. A., Amara, J., Komba, T., Laar, C., Sesay, A., Derkyi, N. S., & Frazer-williams, R. (2023). Seasonal assessment of heavy metal contamination of groundwater in two major dumpsites in Sierra Leone. *Cogent Engineering*, *10*(1), 1–30. https: //doi. org/10. 1080/23311916. 2023.2185955

Scherer, T. (2019). *WQ1030 Iron and Manganese Removal Iron and Manganese Removal*. *1030*(May), 1–8. www.ag.ndsu.edu/publica

Schröder, N., Figueiredo, L. S., & De Lima, M. N. M. (2013). Role of brain iron accumulation in cognitive dysfunction: Evidence from animal models and human studies. *Journal of Alzheimer's Disease*, *34*(4), 797–812. https://doi.org/10.3233/JAD-121996

Sharma, S. K., Petrusevski, B., & Schippers, J. C. (2005). Biological iron removal from groundwater: A review. *Journal of Water Supply: Research and Technology - AQUA*, *54*(4), 239–247. https://doi.org/10.2166/aqua.2005.0022

Sheskin, D. J. (2020). The Mann–Whitney U Test. *Handbook of Parametric and Nonparametric Statistical Procedures*, 531–594. https://doi.org/10.1201/9780429186196-17

Siddiq, O. M., Tawabini, B. S., Soupios, P., & Ntarlagiannis, D. (2022). Removal of arsenic from contaminated groundwater using biochar: A technical review. *International Journal of Environmental Science and Technology*, *19*(1), 651–664. https://doi.org/10.1007/s13762-020-03116-x

Tabassum, R. A., Shahid, M., Niazi, N. K., Dumat, C., Zhang, Y., Imran, M., Bakhat, H. F., Hussain, I., & Khalid, S. (2019). Arsenic removal from aqueous solutions and groundwater using agricultural biowastes-derived biosorbents and biochar: A column-scale investigation. *International Journal of Phytoremediation*, *21*(6), 509–518. https: //doi. org/10. 1080/15226514.2018.1501340

Tan, X. F., Zhu, S. S., Wang, R. P., Chen, Y. Di, Show, P. L., Zhang, F. F., & Ho, S. H. (2021). Role of biochar surface characteristics in the adsorption of aromatic compounds: Pore structure and functional groups. *Chinese Chemical Letters*, *32*(10), 2939–2946. https: //doi. org/10.1016/j.cclet.2021.04.059

Taylor, R. (1990). Interpretation of the Correlation Coefficient: A Basic Review. *Journal of Diagnostic Medical Sonography*, *6*(1), 35–39. https://doi.org/10.1177/875647939000600106

TBS. (2018). *Tanzania Standard-TZS 789_2018- EAS 12_ 2018 ICS_ 67.060.pdf*.

Ukah, B. U., Egbueri, J. C., Unigwe, C. O., & Ubido, O. E. (2019). Extent of heavy metals pollution and health risk assessment of groundwater in a densely populated industrial area, Lagos, Nigeria. *International Journal of Energy and Water Resources*, *3*(4), 291–303. https://doi.org/10.1007/s42108-019-00039-3

Un-ei, R. B., Awasaki, N. K., Gata, F. O., & Akamura, T. N. (2006). Removal of Lead and Iron Ions by Vegetable Biomass. *Journal of Oleo Science, 55*(8), 423–427. doi:10.5650/jos.55.423

Usman, U. A., Yusoff, I., Raoov, M., Alias, Y., Hodgkinson, J., Abdullah, N., & Hussin, N. H. (2021). Natural sources of iron and manganese in groundwater of the lower Kelantan River Basin, North-eastern coast of Peninsula Malaysia: Water quality assessment and an adsorption-based method for remediation. *Environmental Earth Sciences*, *80*(12). https://doi.org/10.1007/s12665-021-09717-0

Verma, L., & Singh, J. (2019). Synthesis of novel biochar from waste plant litter biomass for the removal of Arsenic (III and V) from aqueous solution: A mechanism characterization, kinetics and thermodynamics. *Journal of Environmental Management*, *248*(July), 109235. https://doi.org/10.1016/j.jenvman.2019.07.006

Vunain, E., Kenneth, D., & Biswick, T. (2017). Synthesis and characterization of low-cost activated carbon prepared from Malawian baobab fruit shells by H3PO4 activation for removal of Cu(II) ions: equilibrium and kinetics studies. *Applied Water Science*, *7*(8), 4301–4319. https://doi.org/10.1007/s13201-017-0573-x

Vunain, E., Mishra, A. K., & Krause, R. W. (2013). Ethylene-vinyl acetate (EVA)/polycaprolactone (PCL)-Fe3O 4 composites: Preparation, thermal and mechanical properties. *Journal of Thermal Analysis and Calorimetry*, *114*(2), 791–797. https://doi.org/10.1007/s10973-013-3004-8

Wang, Y., Sikora, S., Kim, H., Boyer, T. H., Bonzongo, J. C., & Townsend, T. G. (2013). Effects of solution chemistry on the removal reaction between calcium carbonate-based materials and Fe(II). *Science of the Total Environment*, *443*, 717–724. https: //doi. org/10. 1016/j.scitotenv.2012.11.009

Wang, Y., Zheng, C., & Ma, R. (2018). Review: Safe and sustainable groundwater supply in China. *Hydrogeology Journal*, *26*(5), 1301–1324. https://doi.org/10.1007/s10040-018-1795-1

WHO. (2011). *Guidelines for Drinking-water Quality. 4th Edition. 978 92 4 154815 1*. World Heath Organization. Geneva, Switzerland. https: //www. who. int/ publications/ i/item /9789241549950

Wu, J., Li, P., Wang, D., Ren, X., & Wei, M. (2020). Statistical and multivariate statistical techniques to trace the sources and affecting factors of groundwater pollution in a rapidly growing city on the Chinese Loess Plateau. *Human and Ecological Risk Assessment*, *26*(6), 1603–1621. https://doi.org/10.1080/10807039.2019.1594156

Zhai, Y., Han, Y., Xia, X., Li, X., Lu, H., Teng, Y., & Wang, J. (2021). Anthropogenic organic pollutants in groundwater increase releases of fe and mn from aquifer sediments: Impacts of pollution degree, mineral content, and ph. *Water (Switzerland)*, *13*(14). https://doi.org/10.3390/w13141920

Zhang, X., He, J., He, B., & Sun, J. (2019). Assessment, formation mechanism, and different source contributions of dissolved salt pollution in the shallow groundwater of Hutuo River

alluvial-pluvial fan in the North China Plain. *Environmental Science and Pollution Research*, *26*(35), 35742–35756. https://doi.org/10.1007/s11356-019-06502-2

RESEARCH OUTPUTS

(i)   Research Paper

Mkelemi, M. J., Mwaijengo, G. N., & Rwiza, M. J. (2024). Assessment of Physicochemical Profile and Heavy Metal Constituents in the Groundwaters of Rural Areas in Southwest Tanzania. *Water Resources*, *51*(4), 562–575. https://doi.org/10.1134/S0097807823602765

(ii)   Poster Presentation